Astrophysical limit on the coupling constant of hypothetical leptonic photons to leptons

B. V. Martemyanov
Institute for Theoretical and Experimental Physics, 117218 Moscow, Russia

(Submitted 23 July 1999)
Pis'ma Zh. Éksp. Teor. Fiz. **70**, No. 5, 321–322 (10 September 1999)

The hypothetical leptonic photons, namely, those that have coupling to electrons, can be produced in the Sun and other stellar objects by the process of photoproduction. Being weakly interacting particles they could substantially influence the evolution of the star by changing the process of heat release. In order for this not to happen, the leptonic coupling constant must be smaller than $\sim 10^{-26}$, i.e., much smaller than the $\sim 10^{-12}$ required for the stability of bodies against the leptonic Coulomb forces. © *1999 American Institute of Physics.*
[S0021-3640(99)00117-6]

PACS numbers: 14.70.Bh, 14.80.−j, 96.60.Vg, 95.30.Cq

Leptonic charges are conserved to the present experimental knowledge. The electronic, muonic, and tauonic lepton numbers are separately conserved. This allows one to couple massless particles to each of these conserved charges.[1] Doing so gives rise to new long-range forces, the most important of which for terrestrial phenomena is the long-range force between electrons due to the electronic Coulomb interaction. The unscreened leptonic charge of electrons in bodies is limited to a very high degree by Eötvös-like experiments, and the electronic coupling constant must be smaller than $\sim 10^{-49}$ in this case.[2] Thus the situation with unscreened electronic charge is uninteresting because it requires an extremely small coupling constant ($\sim 10^{-49}$) that cannot be measured in any other experiments. The electronic charge cannot be screened by antileptonic charge of antineutrinos,[3] since the outward pressure of antineutrinos will break up any body to small pieces of a size $\sim a(\alpha/\sqrt{\alpha_l}) \sim 10^{-4}$ cm (for $\alpha_l \sim 10^{-12}$; Ref. 3). Here $a \sim 10^{-8}$ cm is the dimension of an atom, α is the fine-structure constant, and α_l is the electronic charge coupling constant. The number $\alpha_l \sim 10^{-12}$ is the experimental upper limit for α_l. The electronic charge could be screened by scalar particles with antielectronic charge, e.g., supersymmetric partners of antineutrinos, if they are sufficiently light, say with a mass of about 1 eV.[3] In this case the electronic coupling constant is limited at the level $\alpha_l < \alpha^6 \sim 10^{-12}$ (Refs. 4 and 5) by the requirement of mechanical stability of the skin layer of bodies. It seems plausible that other terrestrial physical phenomena (like surface tension, for example) could improve this limit. But there is a well-known extraterrestrial phenomenon (the Sun) that improves the limit up to $\alpha_l \lesssim 10^{-26}$, i.e., fourteen orders of magnitude. In the present note we will discuss this new limit obtained from the considerations of possible energy losses by the Sun due to emission of leptonic photons.

The Sun is emitting photons coupled to the electric charge. Photons are produced in the hot ($T_i \sim 15\times 10^6$ °C) central part of the Sun and diffuse to the outer layers of the Sun in about $R^2/\lambda c \sim 10^{11}$ s. Here $R \sim 6\times 10^{10}$ cm is the radius of the Sun, $\lambda \sim 1$ cm is the mean free path of the photons in the inner layers of the Sun, and $c = 3\times 10^{10}$ cm/s is the speed of light. The photons that are emitted from the Sun comes from the photosphere of the Sun and have a blackbody spectrum with a temperature $T_e \sim 6\times 10^3$ °C. Thus, the photon luminosity of the Sun is proportional to $T_e^4 R^2$. Leptonic photons can be produced in the Sun by the process $\gamma e \to \gamma_l e$. The mean free path of leptonic photons is determined by the reverse process $\gamma_l e \to \gamma e$ and can be easily compared to the mean free path of the photons determined by the Compton scattering on electrons, $\gamma e \to \gamma e$. Because of the obvious similarity of the above processes we have for the mean free path of leptonic photons $\lambda_l = (\alpha/\alpha_l)\lambda$. If $\alpha_l \sim 10^{-12}$, then $\lambda_l \sim 10^{10}$ cm$\sim (1/6)R$. Thus leptonic photons scatter on the order of $(R/\lambda_l)^2 \sim 36$ times in the Sun and are emitted from a depth $\sim (1/6)R$, where they have a temperature close to $T_i \gg T_e$. The luminosity of leptonic photons $\sim T_i^4 R^2$ is many orders of magnitude larger than the photon luminosity $\sim T_e^4 R^2$. Therefore the case $\alpha_l \sim 10^{-12}$ is strongly ruled out.

If $\lambda_l > R$ (this requires that $\alpha_l < 10^{-13}$), leptonic photons are emitted from the Sun without scattering. Let us calculate the luminosity of the Sun in leptonic photons in this case. The number of leptonic photons emitted from a unit volume per unit time is equal to

$$\sigma_{\gamma e \to \gamma_l e} \cdot n_e \cdot n_\gamma = \frac{n_\gamma}{\lambda_l} \sim \frac{T_i^3}{\lambda_l}.$$

They have the energy $\sim T_i$. The luminosity considered is then proportional to $\sim (T_i^4/\lambda_l)R^3$. It must be small compared to the photon luminosity $\sim T_e^4 R^2$. Therefore we should have $\lambda_l \gg (T_i^4/T_e^4)R \sim 10^{24}$ cm and consequently $\alpha_l \ll 10^{-24}\alpha \sim 10^{-26}$. This is the desired limit on the leptonic coupling constant imposed by what we know about the energy losses of the Sun. Other stars like red supergiants certainly improve this limit as they do for other weakly interacting particles,[6,7] but even at the present limit $\alpha_l \ll 10^{-26}$ all terrestrial problems with leptonic photons and leptostatic repulsion seem to be forgotten. In particular, the critical size of a body with unscreened leptonic charge is $\sim a(\alpha/\sqrt{\alpha_l}) \sim 10^3$ cm, while the size of the skin layer is $\sim a/\sqrt[3]{\alpha_l} \sim 5$ cm (Ref. 4). This means that bodies are quite stable against leptonic forces.

Thus we conclude that the leptonic coupling constant is limited by the known energy losses of the Sun at the level $\sim 10^{-26}$. This limit can be improved by red supergiants. Terrestrial experiments with leptonic photons are highly questionable.

[1] L. B. Okun, Phys. Lett. B **382**, 389 (1996).
[2] L. B. Okun, ''A remark on leptonic photons,'' June 1972 (Manuscript in Russian presented at the ITEP theoretical seminar).
[3] S. I. Blinnikov, A. D. Dolgov, L. B. Okun, and M. B. Voloshin, Nucl. Phys. B **458**, 52 (1996).
[4] B. V. Martemyanov, JETP Lett. **66**, 547 (1997).
[5] B. V. Martemyanov, JETP Lett. **68**, 14 (1998).
[6] M. I. Vysotskiĭ, A. D. Dolgov, and Ya. B. Zel'dovich, JETP Lett. **26**, 188 (1977).
[7] H. M. Georgi and S. L. Glashow, Nucl. Phys. B **193**, 297 (1981).

Published in English in the original Russian journal. Edited by Steve Torstveit.

Localization and channeling of light in defect modes of two-dimensional photonic crystals

A. M. Zheltikov, S. A. Magnitskiĭ, and A. V. Tarasishin
M. V. Lomonosov Moscow State University, 119899 Moscow, Russia

(Submitted 26 July 1999)
Pis'ma Zh. Éksp. Teor. Fiz. **70**, No. 5, 323–328 (10 September 1999)

The spatial distribution of the electromagnetic field in a two-dimensional photonic crystal with a lattice defect is investigated. It is shown that in such a structure the field can be localized in a region smaller than one wavelength in size. The dependence of the spectrum of defect modes on the parameters of a two-dimensional photonic crystal is investigated. The light field at the exit of the photonic crystal possesses properties of a nonradiative mode, making it possible to achieve spatial resolution in the near-field much higher than the radiation wavelength. The possibilities of using this phenomenon in optical near-field microscopy to produce optical memory devices and to increase the efficiency of nonlinear optical interactions are discussed.
 [S0021-3640(99)00217-0]

PACS numbers: 42.70.Qs, 42.65.Wi, 61.72.−y

Localization of an electromagnetic field is one of the important properties of structures with photonic band gaps (PBGs).[1] Such effects in photonic crystals have been widely investigated previously on the basis of analysis of the dispersion properties of PBG structures,[2] where the basic properties of the transmission spectrum of a PBG structure were established, and by various modifications of the slowly varying amplitude approximation,[3] which made it possible to understand the basic mechanisms of localization of the field of a plane wave with a slowly varying envelope in one-dimensional photonic crystals. Recent experiments[4] indicate the possibility of obtaining channeling and rotation (including by large angles) of light beams in two-dimensional PBG structures containing defects of the photonic crystal lattice. Such effects cannot be understood physically by analyzing the dispersion properties of PBG structures or on the basis of the plane-wave approximation, since such approaches do not permit determining the field in a photonic crystal. At the same time, the problem of describing the field of light waves analytically in and at the exit from two- and three-dimensional PBG structures is hardly solvable. Numerical simulation methods seem to offer the only possibility of investigating the distribution of the field in such structures.

An approach based on the numerical solution of Maxwell's equations by the finite-difference time-domain (FDTD)[5] method appears to hold promise for investigating the field distribution in PBG structures. This technique has been used successfully to study optical confinement[6] and the formation of extremely short light pulses in one-dimensional

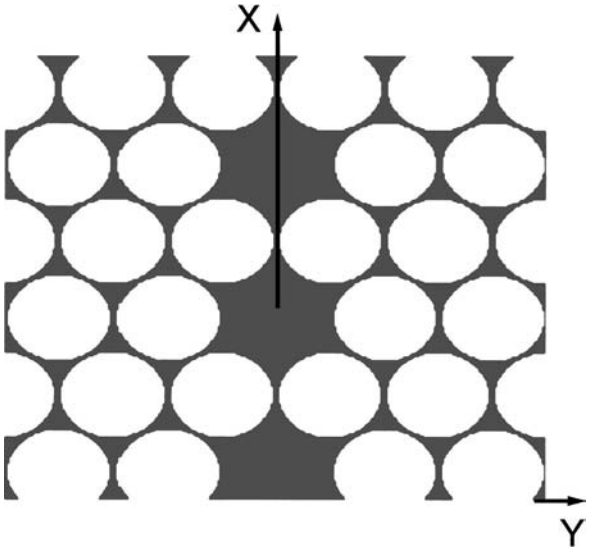

FIG. 1. Fragment of a two-dimensional PBG structure with a lattice defect.

PBG structures.[7] In the present letter the FDTD method is used to analyze localization and channeling of an electromagnetic field in a two-dimensional PBG structure with a lattice defect. The wideband test-pulse method is used to calculate the spectrum of defect modes in the band gaps of photonic crystals. This approach makes it possible to draw physically and technically important conclusions about the character of light channeling in defect modes of PBG structures. The analysis performed in the present work shows that under these conditions an electromagnetic field can be localized in a region smaller than one wavelength in size, and the field at the exit of a PBG structure possesses the properties of a nonradiative mode. It is shown that the spectrum of defect modes can be controlled by varying the parameters of the PBG structure.

To study the localization and channeling of light in a two-dimensional PBG structure with a lattice defect we solved Maxwell's equations numerically by the finite-difference method. The field incident on the boundary of a PBG structure had the form of a plane wave. The absorbing Neumann boundary conditions[8] used in this method made it possible to avoid effects due to reflections from artificial boundaries. A structure consisting of a variable number of periods (from 5 to 10) of cylindrical air gaps, forming a triangular lattice in a silicon matrix, was chosen as the object of investigation (Fig. 1). This choice of the type of photonic crystal is based on the fact that silicon technologies are very promising for preparing one-,[9] two-,[10] and three-dimensional[11] PBG structures. Numerical calculations for the defect-free PBG structure described above showed the existence of a gap for the direction along the X axis (Fig. 1), which corresponds to the minimum gap width,[12] for the ratio a/λ (where a is the period of the PBG structure and λ is the wavelength of the light beam) varying from 0.35 to 0.52 for H (TE) modes and from 0.44 to 0.57 for E (TM) modes. Thus, the results of our calculations indicate the existence of a closed band gap and are in good agreement with calculations performed in

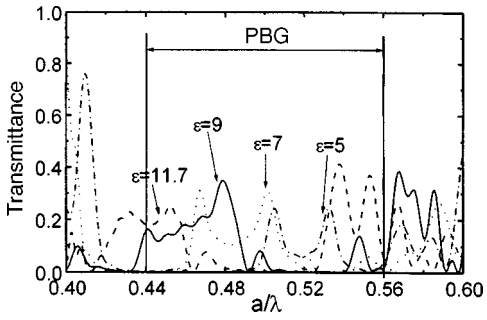

FIG. 2. Spectrum of defect modes of a two-dimensional PBG structure, a fragment of which is shown in Fig. 1, for various dielectric constants of the matrix material: ϵ=11.7 (dashed line), 9 (solid line), 7 (dotted line), and 5 (dot-and-dash line).

Ref. 12 by the plane-wave method as well as with the results of calculations and experiments reported in Ref. 10.

To introduce a defect into the two-dimensional PBG structure described above, one row of air pores was removed. Such a lattice defect was introduced, with a period Λ along the Y axis (Fig. 1). The problem of the propagation of a light beam in such a two-dimensional PBG structure with a defect makes it possible to give a full assessment of the advantages of the numerical analysis scheme, where the introduction of a defect, in contrast to the widely used plane-wave method, does not greatly complicate the procedure. Numerical analysis shows that if the intensity of the field in a PBG structure with no defect decays on a spatial scale of the order of the radiation wavelength λ and the PBG structure is characterized by a transmission coefficient of the order of 10^{-3}, then a light beam can propagate in the PBG structure with a defect only along a narrow channel formed by the defect. The transmission coefficient for E modes with a/λ from 0.44 to 0.47 in such a structure increases from 10^{-3} to 0.5, attesting to the appearance of a defect level in the band gap. The spectrum of defect modes for propagation along the X axis for E modes is shown in Fig. 2. This spectrum was calculated by the wideband test-pulse method, i.e., the propagation of a short pulse with a wide spectrum, greater than the spectral range under investigation, through a two-dimensional PBG structure with a lattice defect was simulated. The Fourier transform of the spectrum of such a pulse at the exit of the PBG structure with a defect made it possible to find the spectrum of the defect modes. Analysis of the transmission spectrum of the PBG structure with a defect shows that the spectrum of defect modes can be controlled by varying the parameters of the photonic crystal. As one can see from Fig. 2, as the ratio of the refractive index of the matrix material to the refractive index of the material of the cylinders (in our case, air) decreases, the defect modes of the PBG structure shift to higher frequencies. This phenomenon can be clearly interpreted on a qualitative level by representing the defect mode of the PBG structure as a standing wave formed as a result of reflection from the walls of the channel formed by the defect. Then the wave number of such a standing wave decreases with increasing ratio of the refractive indices of the materials forming the PBG structure.

Figure 3 shows the two-dimensional distribution of the mean-square electric field $\overline{E^2}$ in a PBG structure of the type described above, consisting of ten periods along the X axis

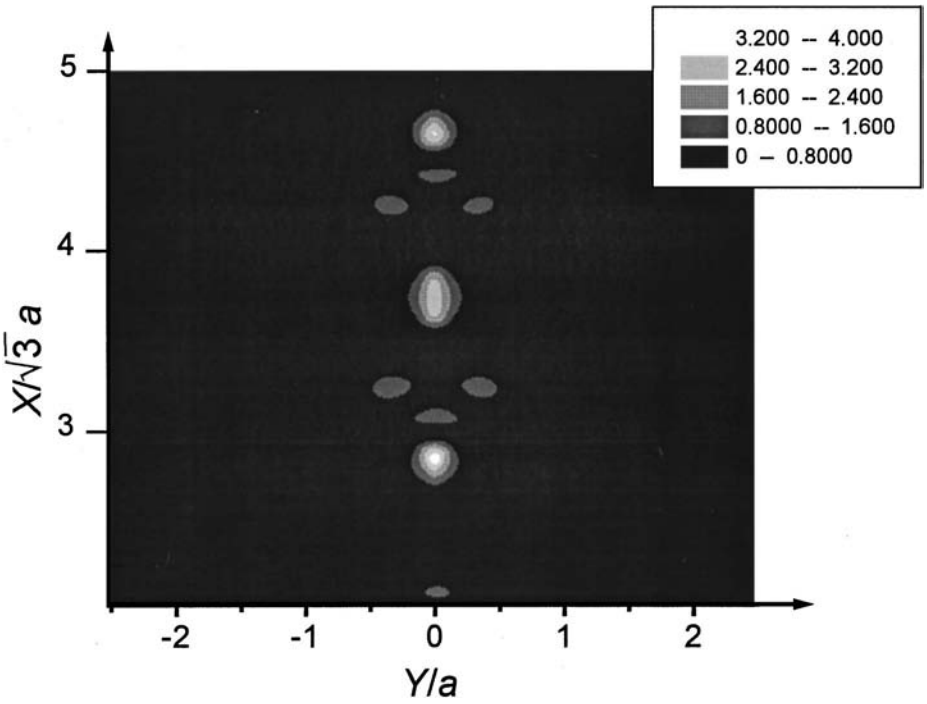

FIG. 3. Two-dimensional plot of the localization of an electric field in a PBG structure with a lattice defect (a fragment of this structure is shown in Fig. 1). The gray tones represent the mean-square electric field $\overline{E^2}$ for a ratio $a/\lambda = 0.454$.

with defect period $\Lambda = 5a$, for $a/\lambda = 0.454$. Analysis of the spatial distribution of the electromagnetic field shows that light is channeled along the defect in this structure, and the field is localized at the center of the defect. For certain sections of the channel the beam diameter is of the order of $\lambda/10$ (Fig. 3), which is five times smaller than the diffraction limit for a light beam focused in air. The light intensity at the center of the defect is several hundreds of times greater than the intensity at the channel edges (Fig. 3). This attests to a high contrast of the beam channeling. The group velocity of the light decreases substantially, indicating the possibility of using defect modes of PBG structures to produce controllable optical delay lines, similarly to the optical delay lines based on one-dimensional PBG structures which were produced in Ref. 13. Light channeling along a defect was observed independently of the period Λ with which the defect was introduced. This shows that the light-localization phenomena described above are not due to interference of the light reflected from neighboring defects. Beyond the photonic crystal and far from its surface the field intensity integrated over a period Λ remained constant independent of the value of Λ. This shows that the light is channeled only along a given defect.

The distribution of the mean-square electric field at the exit of the PBG structure is presented in Fig. 4. Under these conditions the field is localized in the transverse direction on a spatial scale less than the radiation wavelength ($\lambda/10$), decaying exponentially along the X axis. The properties of this field are similar to those of a nonradiative mode

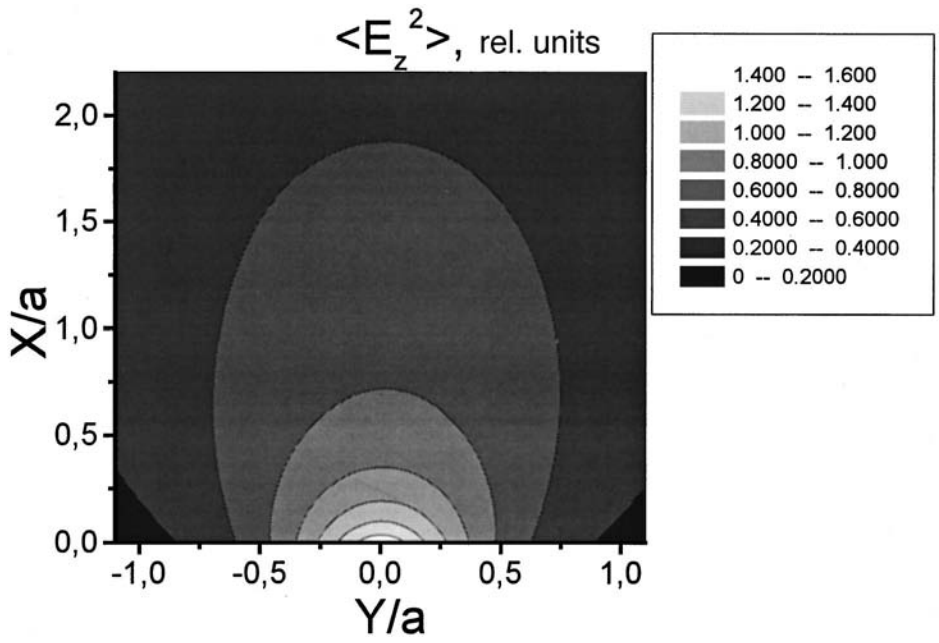

FIG. 4. Two-dimensional plot of the distribution of the mean-square electric field at the exit of a PBG structure with a lattice defect (a fragment of the structure is shown in Fig. 1) for $a/\lambda = 0.454$.

localized near the surface of a sample in near-field microscopy. This opens up the possibility of using PBG structures in optical near-field microscopy,[14] as components that effectively form nonradiative modes. Using the reciprocity principle, we find that PBG structures with a lattice defect can also be used to analyze the nonradiative field near a sample, making it possible to implement a data-acquisition mode in near-field microscopy.

It is extremely unlikely that an analytical description can be found for the field at the exit of PBG structures of the type under study. However, on the basis of qualitative physical considerations it is obvious that a light beam less than one wavelength in diameter in a two-dimensional photonic crystal cannot propagate in free space without a change in form. Since the diameter of such a beam is much less than the wavelength and the spectrum of the beam contains spatial harmonics of high orders, such a beam exhibits properties similar to those of nonradiative modes. Such a beam gives high resolution in the near field and decays rapidly in the longitudinal direction (along the X axis). Even though in this case all of the energy propagates along the exit surface of the PBG structure, the high density of the light field at the exit of such a structure can lead to physically observable phenomena in the near zone. This field can be used, specifically, for local excitation of atoms or molecules. It can also be detected, similarly to the near-field microscopy scheme, by using a probe located near the surface.

Aside from various near-field microscopy schemes, the light-beam propagation regimes that can be realized with PBG structures hold promise for a variety of applications. Important applications utilizing the properties of the field at the exit of a PBG structure

derive from the possibility of increasing the spatial resolution in photolithography, of increasing the information storage density in optical-memory systems, and of visualizing the mode composition of radiation in optical waveguides. The possibility of focusing a light beam in a region smaller than one wavelength in size opens up new possibilities for increasing the information storage density in three-dimensional optical memory systems.[15] The fact, established in the present work, that there is no interference of radiation propagating in neighboring defects in a PBG structure is extremely important. This circumstance makes it possible to obtain high locality of information writing and reading without disturbing the information stored in neighboring three-dimensional memory cells. Finally, the possibility of a local increase in the field over quite extended spatial scales in the direction of propagation of a light beam holds promise for increasing the efficiency of nonlinear optical interactions. However, nonlinear propagation regimes of light beams in two- and three-dimensional photonic crystals require additional study, the results of which we hope to report in subsequent publications.

In summary, the above analysis of the propagation of electromagnetic fields in two-dimensional PBG structures with a lattice defect and the investigation of the spectrum of defect modes in the gaps of such structures have revealed a number of important properties of field localization in photonic crystals. Under these conditions a light field can be localized in a region smaller than one wavelength in size, and the field at the exit of the PBG structure possesses properties of a nonradiative mode, which makes it possible to achieve spatial resolution in the near field much higher than one wavelength of the radiation. The light-beam propagation regimes that can be obtained with PBG structures hold promise for solving a variety of problems of near-field optical microscopy, for increasing the density of information storage in optical memory devices, and for increasing the efficiency of nonlinear optical interactions.

We shall always treasure the memory of many discussions with and the invaluable support of this work by N. I. Koroteev, who passed away suddenly. N. I. Koroteev initiated our investigations in the field of photonic crystals.

This research was supported by the Constellation Group GmbH. The research of A. M. Zh. and A. V. T. was supported in part by INTAS Grant 97-0369.

[1] J. Joannopoulos, R. Meade, and J. Winn, *Photonic Crystals* (Princeton University Press, Princeton, 1995).
[2] D. R. Smith, R. Dalichaouch, N. Kroll *et al.*, J. Opt. Soc. Am. B **10**, 314 (1993); A. Figotin and A. Klein, J. Opt. Soc. Am. A **15**, 1423 (1998).
[3] M. Scalora, M. J. Bloemer, A. S. Manka *et al.*, Phys. Rev. A **56**, 3166 (1997).
[4] S.-Y. Lin, E. Chow, V. Hietala *et al.*, Science **282**, 274 (1998).
[5] A. Taflove, *Computational Electrodynamics: The Finite-Difference Time-Domain Method* (Artech House, Norwood, Mass., 1995).
[6] P. Tran, Opt. Lett. **21**, 1138 (1996).
[7] N. I. Koroteev, S. A. Magnitskii, A. V. Tarasishin, and A. M. Zheltikov, Opt. Commun. **159**, 191 (1999).
[8] B. Engquist and A. Majda, Math. Comput. **31**, 629 (1977).
[9] L. A. Golovan', A. M. Zheltikov, P. K. Kashkarov *et al.*, JETP Lett. **69**, 300 (1999).
[10] U. Gruening, V. Lehmann, S. Ottow, and K. Busch, Appl. Phys. Lett. **68**, 747 (1996).
[11] J. G. Fleming and S.-Y. Lin, Opt. Lett. **24**, 49 (1999).
[12] R. D. Meade, K. D. Brommer, A. M. Rappe, and J. D. Joannopoulos, Appl. Phys. Lett. **61**, 495 (1992).
[13] M. Scalora, R. J. Flynn, S. B. Reinhardt *et al.*, Phys. Rev. E **54**, R1078 (1996).
[14] M. A. Paesler and P. J. Moyer, *Near-Field Optics* (Wiley, New York, 1996).
[15] D. A. Akimov, A. B. Fedotov, N. I. Koroteev *et al.*, Jpn. J. Appl. Phys., Part 1 **36**, Part 1, 1B, 426 (1997).

Translated by M. E. Alferieff

A new optical method for measuring the electron–phonon interaction parameter $\lambda\langle\Omega^2\rangle$ using the spectral dependence of the relaxation rate

A. L. Dobryakov and Yu. E. Lozovik*)
Spectroscopy Institute, Russian Academy of Sciences, 142092 Troitsk, Moscow District, Russia

(Submitted 9 August 1999)
Pis'ma Zh. Éksp. Teor. Fiz. **70**, No. 5, 329–332 (10 September 1999)

The spectral dependence of the electron–phonon relaxation rate $\gamma_{e-ph}(\hbar\omega)$ in metals is studied in pump–supercontinuum-probe (PSCP) experiments with femtosecond time resolution. Investigation of this spectral dependence, which exhibits a substantial slowing of the relaxation rate $\gamma_{e-ph}(\hbar\omega)$ near the Fermi level E_F, using the parametrization $\gamma_{e-ph}(\hbar\omega)\propto\lambda\langle\Omega^2\rangle(\hbar\omega-E_F)^2$ makes it possible to determine directly the electron–phonon interaction parameter $\lambda\langle\Omega^2\rangle$. The parameter $\lambda\langle\Omega^2\rangle$ for $YBa_2Cu_3O_{7-\delta}$ is analyzed using this method. [S0021-3640(99)00317-5]

PACS numbers: 78.47.+p, 63.20.Kr, 74.25.Jb, 74.25.Kc, 74.72.Bk

It is of interest to study the electron–phonon interaction in metals and superconductors because it plays the governing role in such fundamental physical phenomena as superconductivity and transport processes in metals (see, for example, the reviews in Refs. 1–3). The principal mechanisms of charge-carrier scattering in metals, semimetals, and semiconductors and, in particular, the electron–phonon interaction are elucidated in detail in the monograph by Gantmakher and Levinson,[4] along with a discussion of the modern advances in the kinetics of current carriers and the basic experiments in which the effects of this scattering are strongest. In the present letter we consider only the electron–phonon scattering mechanism.

The many-body theory of the electron–phonon interaction, describing both normal and superconducting states of a metal, is ultimately expressed in terms of the spectrum densities of the electron-phonon interaction. One such function — the Éliashberg function $\alpha^2(\Omega)F(\Omega)$, describing the change in the single-particle properties of electrons in the normal state and the phonon contribution to superconductivity — can be determined experimentally from data on the dependence of the tunneling current between a normal metal and a superconductor on the applied voltage,[3] though it is very difficult to determine for anisotropic superconductors and superconductors with a short coherence length. An alternative approach to determining $\alpha^2(\Omega)F(\Omega)$ or related functions, specifically, the electron–phonon interaction parameter $\lambda\langle\Omega^2\rangle$, from the rate of change of the effective temperature T_e of the electronic subsystem[5] involves the use of femtosecond spectroscopy.[6] This approach has been used to determine the parameter $\lambda\langle\Omega^2\rangle$ in high-

temperature superconductors and metals[6,7] (Cu, Au, Nb, and so on).

As will be shown below, there is a more accurate method for determining the parameter $\lambda\langle\Omega^2\rangle$, based on femtosecond-resolution pump–supercontinuum-probe (PSCP) spectroscopy,[7–9] which makes it possible to determine the spectral dependence of the electron–phonon relaxation rate $\gamma_{e-ph}(\hbar\omega)$. A characteristic feature of the spectral dependence $\gamma_{e-ph}(\hbar\omega)$ is that the relaxation rate decreases near the Fermi level E_F.[7,10] As will be shown below, near E_F the spectral dependence $\gamma_{e-ph}(\hbar\omega)$, describing the relaxation of electrons after laser pumping, is determined by the expression $\gamma_{e-ph}(\hbar\omega) \propto \lambda\langle\Omega^2\rangle(\hbar\omega - E_F)^2$, which makes it possible to determine the parameter $\lambda\langle\Omega^2\rangle$.

Let us examine the basic physical processes involved in the excitation of a metal (superconductor) by an ultrashort laser excitation pulse. The excitation pulse (with duration τ_{pu}) is absorbed by free electrons in the conduction band. This creates a nonequilibrium distribution of the electronic subsystem. The electron–electron interaction determines the establishment, on a femtosecond time scale, of a quasiequilibrium distribution of the electronic subsystem (with an effective electron temperature T_e greater than the lattice temperature T_L) with characteristic relaxation rate γ_{ee}. Next (at times $t \gg \tau_{pu}$, γ_{ee}^{-1}), the electron–phonon interaction equalizes the electron and the lattice temperatures with a characteristic relaxation rate γ_{e-ph}. A probe laser pulse is used to probe the absorption due to transitions from a deep-lying filled band near E_F in the conduction band; this gives a sign-alternating difference absorption spectrum[6,7] with passage through zero at the point corresponding to interband transitions near E_F. Measurement of the kinetics of reflection and transmission by femtosecond spectroscopy methods makes it possible to determine the cooling rate γ_T of the electronic subsystem,[5] which is related with the parameter $\lambda\langle\Omega^2\rangle$, as

$$\partial T_e/\partial t = \gamma_T(T_L - T_e), \quad \gamma_T = 3\hbar\lambda\langle\Omega^2\rangle/\pi k_B T_e, \tag{1}$$

where k_B is Boltzmann's constant and $\hbar$ is Planck's constant. The parameter $\lambda\langle\Omega^2\rangle$ plays an important role in the theory of superconductivity, and the most direct method for measuring this parameter can be implemented using femtosecond laser spectroscopy. This approach was used to determine $\lambda\langle\Omega^2\rangle$ from femtosecond spectroscopy data: The parameter $\lambda\langle\Omega^2\rangle$ was determined from the rate of change of the effective electronic temperature T_e [see Eq. (1)] for metals[6] (Cu, Au, Nb) and a number of high-temperature superconductors[6,7] ($YBa_2Cu_3O_{7-\delta}$, $BiSr_2CaCu_2O_{8+x}$). It should be noted that this approach neglects the spectral dependence of the electron–phonon relaxation rate (see below), and it can therefore be regarded only as an estimate of the electron–phonon interaction parameter $\lambda\langle\Omega^2\rangle$. We shall show that the parameter $\lambda\langle\Omega^2\rangle$ can be determined by investigating the spectral dependence of the electron–phonon relaxation rate using femtosecond PSCP spectroscopy.[7–9]

A many-body electron–phonon interaction theory is presented in a number of reviews,[1,2] and we shall not examine this theory in detail here. We shall present only the basic relations that will be needed below. The electronic self-energy $\Sigma(\omega)$ can be calculated taking account of very simple contributions of first-order in electron–phonon interaction. Higher-order terms can be neglected, because they are small in the ratio[1,2] ω_D/E_F. Here ω_D is the characteristic phonon frequency and E_F is the Fermi energy. The self-energy $\Sigma(\omega)$ has real and imaginary parts. The imaginary part characterizes the electron–phonon relaxation rate $\gamma_{e-ph}(\omega, T_L, T_e)$:

$$\gamma_{e-ph}(\omega,T_L,T_e)=2\pi\int d\Omega\,\alpha^2(\Omega)F(\Omega)[2n(\Omega,T_L)+1]$$
$$-2\pi\int d\Omega\,\alpha^2(\Omega)F(\Omega)\frac{\sinh(\hbar\Omega/k_BT_e)}{\cosh[(\hbar\omega-E_F)/k_BT_e]+\cosh[\hbar\Omega/k_BT_e]}, \tag{2}$$

where $n(\Omega,T_L)$ is the Bose distribution function, T_e is the effective temperature of the electronic subsystem, T_L is the lattice temperature, and $\alpha^2(\Omega)F(\Omega)$ is the spectral electron–phonon interaction density or the Eliashberg function. We note that the approach of Ref. 4, based on the concept of a test particle, makes it possible to obtain the same expression for $\gamma_{e-ph}(\omega,T_L,T_e)$ using a simpler mathematical apparatus.

In the low-temperature limit, i.e., for temperatures $T_e\ll\hbar\omega_{ph}$, where $\hbar\omega_{ph}$ is the characteristic phonon energy, the spectral density of the electron–phonon relaxation rate near the Fermi level is well known and has the form[4] $\gamma_{e-ph}\sim(\hbar\omega-E_F)^3$, where the proportionality coefficient is not directly related with the electron–phonon interaction parameter $\lambda\langle\Omega^2\rangle$. However, under the conditions of a femtosecond PSCP experiment[6,7,10] the opposite limiting case of high temperatures obtain (with intense pumping), i.e., the effective temperature T_e of the electronic subsystem is much higher than the characteristic phonon frequencies $\hbar\omega_{ph}$. In this limiting case, i.e., when $\hbar\Omega/k_BT_e\ll1$, the electron–phonon relaxation rate $\gamma_{e-ph}(\omega,T_L,T_e)$ is proportional to the electron–phonon interaction parameter $\lambda\langle\Omega^2\rangle$:

$$\gamma_{e-ph}(\omega,T_L,T_e)=\gamma_0(T_L)-\frac{\pi\hbar\lambda\langle\Omega^2\rangle}{2k_BT_e\cosh^2[(\hbar\omega-E_F)/2k_BT_e]}, \tag{3}$$

$$\gamma_0(T_L)=2\pi\int d\Omega\,\alpha^2(\Omega)F(\Omega)[2n(\Omega,T_L)+1],$$

$$\lambda\langle\Omega^2\rangle=2\int d\Omega\,\alpha^2(\Omega)F(\Omega)\Omega.$$

Near the Fermi level $(\hbar\omega-E_F)/2k_BT_e\ll1$ the electron–phonon relaxation rate $\gamma_{e-ph}(\omega,T_L,T_e)$ has the form

$$\gamma_{e-ph}(\omega,T_L,T_e)=a+b(\hbar\omega-E_F)^2, \tag{4}$$

where $a=\gamma_0(T_L)-\pi\hbar\lambda\langle\Omega^2\rangle/2k_BT_e$ and $b=\pi\hbar\lambda\langle\Omega^2\rangle/(2k_BT_e)^3$. It follows from expression (4) that the relaxation rate $\gamma_{e-ph}(\omega,T_L,T_e)$ should decrease near the Fermi level, and we can determine the parameter b and therefore the electron–phonon interaction parameter $\lambda\langle\Omega^2\rangle=b(2k_BT_e)^3/\pi\hbar$ by studying the spectral dependence of the relaxation rate $\gamma_{e-ph}(\omega,T_L,T_e)$.

As already mentioned above, the spectral dependence of the relaxation rate $\gamma_{e-ph}(\omega,T_L,T_e)$ can be investigated by femtosecond PSCP spectroscopy.[7–10] The use of a supercontinuum probe (in the spectral range 1.6–3.2 eV) made it possible to investigate the spectral dependence $\gamma_{e-ph}(\hbar\omega)$ in metal films (Au, Cu) and in high-temperature superconductor films ($YBa_2Cu_3O_{7-\delta}$). The spectral dependence of the relaxation rate $\gamma_{e-ph}(\hbar\omega)$ with a substantial decrease near the Fermi level was observed. This made it possible to determine the position of the Fermi level E_F, i.e., interband transitions from

a low-lying valence band into the region of the Fermi level, which lies in the conduction band, were determined: $E_F = 2.15$ eV for a Cu film, 2.45 eV for a Au film, and 2.09 eV for a $YBa_2Cu_3O_{7-\delta}$ film. We approximated the spectral dependence $\gamma_{e-ph}(\hbar\omega)$ by the function (4), and we obtained the following values for the parameter b: $b_{\mathrm{Cu}} = 45\,\mathrm{ps}^{-1}\cdot\mathrm{eV}^{-2}$, $b_{\mathrm{Au}} = 15\,\mathrm{ps}^{-1}\cdot\mathrm{eV}^{-2}$, and $b_{\mathrm{YBaCuO}} = 290\,\mathrm{ps}^{-1}\cdot\mathrm{eV}^{-2}$. We note the interesting fact that b is much greater for $YBa_2Cu_3O_{7-\delta}$ than for copper and gold.

Now, on the basis of these experimental values, we shall find the electron–phonon interaction parameter $\lambda\langle\Omega^2\rangle = (2k_BT_e)^3/\pi\hbar$. We shall estimate the maximum temperature T_e of the electronic subsystem (assuming that the energy of the excitation pulse is introduced entirely into the electronic subsystem) as $T_e = (1-R)E_{pu}/C_e$, where R is the reflection coefficient, E_{pu} is the energy density of the excitation pulse, and C_e is the electronic specific heat. Under the conditions of the experiment of Ref. 10, $k_BT_{e,\mathrm{Cu}} \sim 0.08$ eV and $k_BT_{e,\mathrm{Au}} \sim 0.1$ eV, which makes it possible to determine the electron–phonon interaction parameter as $\lambda\langle\Omega^2\rangle_{\mathrm{Cu}} \sim 35\,\mathrm{meV}^2$ and $\lambda\langle\Omega^2\rangle_{\mathrm{Au}} \sim 28\,\mathrm{meV}^2$. We note that these values are in good agreement with the values of these parameters determined in previous work from the rate of change of the electron temperature.[6] For a $YBa_2Cu_3O_{7-\delta}$ film the temperature of the electronic subsystem under the conditions of the experiment of Ref. 10 is $k_BT_e \sim 0.26$ eV and the electron–phonon interaction parameter $\lambda\langle\Omega^2\rangle \sim 840\,\mathrm{meV}^2$. We note that this value is different from the value $\lambda\langle\Omega^2\rangle \sim 500\,\mathrm{meV}^2$ obtained previously from the rate of change of the electron temperature.[6] A theoretical estimate[11] of the electron–phonon interaction parameter gives $\lambda\langle\Omega^2\rangle \sim 2200\,\mathrm{meV}^2$. As noted previously, the spectral dependence of the electron–phonon relaxation rate is neglected when the parameter $\lambda\langle\Omega^2\rangle$ is determined from the rate of change of the electron temperature.

In closing, we note that the application of femtosecond PSCP laser spectroscopy makes it possible to determine directly the electron–phonon interaction parameter from the spectral dependence of the electron–phonon relaxation rate. We note that a supercontinuum probe makes it possible to determine the position of the Fermi level according to the decrease in the relaxation rate and to determine the possible deviations of the spectral dependence from the theoretically predicted dependence.

We thank B. F. Gantmakher for a helpful discussion. This work was supported by the Russian Fund for Fundamental Research.

*)e-mail: lozovik@isan.troitsk.ru

[1] P. B. Allen, *Dynamical Properties of Solids*, Vol. 3, edited by G. K. Horton and A. A. Maradudin (North-Holland, Amsterdam, 1980), p. 95.
[2] E. G. Maksimov, D. Yu. Savrasov, and S. Yu. Savrasov, Usp. Fiz. Nauk **167**, 353 (1997).
[3] W. L. McMillan and J. M. Rowell, *Superconductivity*, Vol. 1, edited by R. D. Parks (Dekker, New York, 1969) p. 561.
[4] V. F. Gantmakher and I. V. Levinson, *Scattering of Current Carriers in Metals and Semiconductors* [in Russian] (Nauka, Moscow, 1984).
[5] P. B. Allen, Phys. Rev. Lett. **59**, 1460 (1987).
[6] S. D. Brorson, A. Kazeroonian, E. P. Eppen *et al.*, Phys. Rev. Lett. **64**, 2172 (1990); Solid State Commun. **74**, 1305 (1990).
[7] V. M. Farztdinov, Yu. E. Lozovik, Yu. A. Matveets *et al.*, Phys. Rev. Lett. **67**, 3860 (1991); A. L. Dobryakov, Yu. E. Lozovik, V. M. Farztdinov *et al.*, JETP Lett. **61**, 985 (1995); Yu. E. Lozovik, A. L. Dobryakov, S. A. Kovalenko *et al.*, Phys. Lett. A **223**, 303 (1996).

[8] S. A. Kovalenko, A. L. Dobryakov, J. Ruthmann, and N. P. Ernsting, Phys. Rev. A **59**, 2369 (1999).
[9] V. M. Farztdinov, A. L. Dobryakov, Yu. E. Lozovik *et al.*, Phys. Rev. B **56**, 4176 (1997).
[10] Yu. E. Lozovik, A. L. Dobryakov, V. M. Farztdinov *et al.*, Laser Phys. **9**(2), 557 (1999).
[11] G. L. Zhao and J. Callaway, Phys. Rev. B **49**, 6424 (1994).

Translated by M. E. Alferieff

Quasiclassical description of electronic supershells in simple metal clusters

G. V. Shpatakovskaya
Institute of Mathematical Modeling, Russian Academy of Sciences, 125047 Moscow, Russia

(Submitted 11 August 1999)
Pis'ma Zh. Éksp. Teor. Fiz. **70**, No. 5, 333–337 (10 September 1999)

A quasiclassical method for calculating shell effects, which has been used previously in atomic and plasma physics, is used to describe electronic supershells in metal clusters. An analytical expression is obtained, in the spherical jellium model, for the oscillating part of the binding energy of electrons of a cluster as a sum of contributions from supershells with quantum numbers $2n_r+l$, $3n_r+l$, $4n_r+l$,... This expression is written in terms of the classical characteristics of the motion of an electron with the Fermi energy in a self-consistent potential. The conditions under which a new supershell appears and the relative contribution of this shell are investigated as a function of the cluster size and form of the potential. Specific calculations are performed for a ''square well'' of finite depth. © *1999 American Institute of Physics.* [S0021-3640(99)00417-X]

PACS numbers: 36.40.Cg, 71.18.+y, 61.46.+w

1. The electronic structure of atomic clusters has been intensively studied experimentally and theoretically in the last few years (see, for example, the reviews in Refs. 1 and 2). One characteristic feature of the experimental mass spectra of clusters (the dependence of the number of N-atom clusters on N) is the existence of ''magic'' numbers: Clusters with these numbers of atoms are much more abundant than clusters with the adjacent numbers of atoms. As N increases, this effect diminishes in amplitude, then increases once again, and so on, i.e., oscillations with beats occur. It is known that such effects arise when two or more oscillations are summed. The objective of the present work is to analyze these oscillations in clusters on the basis of a quasiclassical calculation of the shell part of the electron binding energy.

N-atom clusters have been described theoretically, for example, in Ref. 3, on the basis of self-consistent calculations by the density functional method in the jellium model. One result of these works was that the two types of periodicity described above in the N dependence of the oscillatory part $\delta E_{\rm sh}$ of the energy of the electrons in a cluster was obtained: Oscillations with a short period are accompanied by beats whose period is an order of magnitude larger. Similar results have been obtained in Ref. 4 using the phenomenological Woods–Saxon potential and in calculations in Ref. 5 for various metals with nearly self-consistent potentials.

For small clusters, the interpretation of the numerical calculations presents no difficulties: The nonmonotonic dependence of the energy of an electron shell of a cluster on the number of electrons is due to the fact that clusters with completely filled l shells are more stable. However, this law breaks down for $N>100$.

Calculations (see, for example, Ref. 5) show that the energy levels $\varepsilon(n_r,l)$ of electrons in a cluster are grouped in supershells: $\varepsilon(n_r,l)\simeq\varepsilon(n_r+1,l-K)$ with pseudoquantum numbers Kn_r+l, where n_r and l are radial and orbital quantum numbers, $K=2,3,4,\ldots$. For $K=2$ the pseudoquantum number is the same as a principal quantum number and characterizes the arrangement of the single-electron levels in small clusters with $N<100$. As N increases, supershells with $K=3$, followed by $K=4$, and so on appear. By analogy with the theory of Ref. 6 of such effects for a spherical cavity with infinite walls the characteristic oscillations $\delta E_{\rm sh}$ with beats can be attributed to interference of these supershells.[7,8] It is of interest to investigate analytically the origin of supershells and the mechanisms leading to their appearance for a potential of arbitrary form.

In the present letter it is shown that this problem can be solved by a classical method for distinguishing shell effects, previously used successfully in atomic[9,10] and plasma[11,12] physics, on the basis of the Thomas–Fermi (TF) model. This model is valid if the quasiclassicity parameter, which for clusters is proportional to $N^{-1/3}$, is small. Although the TF method itself and its conventional variants with quantum and exchange corrections (for application to clusters, see Refs. 13 and 14) give only the average dependences of all quantities on the number of particles, a refinement of this model makes it possible to take the shell structure of the electronic spectrum of electron–ion systems into account in the quasiclassical approximation. This refinement is based on the use of the Bohr–Sommerfeld quantization conditions and on the possibility of performing the sum over the quantum numbers analytically, provided that the quasiclassicity parameter is small.

2. The exposition below is based on the expression derived in Ref. 9 for the correction to the Thomas–Fermi binding energy of electrons in terms of the correction $\delta n(\mathbf{r})$ to the electron density which because of other effects (exchange, quantum, and so on) goes beyond the TF model:

$$\delta E=\int_{-\infty}^{\mu} d\mu' \int d\mathbf{r}\,\delta n(\mathbf{r},\mu'). \tag{1}$$

Here μ is the chemical potential in the TF model, the integration over $\mathbf{r}$ extends over the entire volume occupied by the system, and the correction $\delta n(\mathbf{r},\mu')$ to the electronic density of states is assumed to be small and is calculated on the basis of the TF potential.

We are interested in the contribution of the shell correction $\delta n_{\rm sh}(\mathbf{r},\mu')$ to the electronic density of states or to the number of states

$$\delta N_{\rm sh}(\mu)=\int d\mathbf{r}\,\delta n_{\rm sh}(\mathbf{r},\mu)=N(\mu)-N_{TF}(\mu), \tag{2}$$

where for a cluster with filled l shells

$$N(\mu)=2\sum_{n_r,l}(2l+1)\,\theta(\mu-\varepsilon_{n_r,l}), \tag{3}$$

and the energy levels $\varepsilon_{n_r,l}$ are determined from the quantization condition

$$S_{\varepsilon l}=\int dr p_{\varepsilon l}(r)=\pi\left(n_r+\frac{1}{2}\right). \tag{4}$$

Here $S_{\varepsilon l}\equiv S_{\varepsilon_\lambda}$ and $p_{\varepsilon l}(r)=\sqrt{2(\varepsilon-U(r))-(l+1/2)^2/r^2}\equiv\sqrt{p_\varepsilon^2(r)-\lambda^2/r^2}\equiv p_{\varepsilon\lambda}$ are, respectively, the classical radial action and momentum of an electron with energy ε and orbital angular momentum l, and the region of integration in the action integral is bounded by the turning points. Simple calculations using the Poisson formula to replace the sum over quantum numbers n_r and l by integrals and switching from integration over n_r to integration over energy ε make it possible to rewrite expression (3) as

$$N(\mu)=\frac{2}{\pi}\sum_{k,s=-\infty}^{\infty}\frac{(-1)^{k+s}}{k}\int_0^{\lambda_\mu}d\lambda\lambda\,\sin(2\pi k\nu_{\mu\lambda})\cos(2\pi s\lambda). \tag{5}$$

Here $\nu_{\varepsilon\lambda}=S_{\varepsilon\lambda}/\pi$, and λ_ε determines the limit of the phase region of the classically allowed motion of an electron with energy ε: $\nu_\varepsilon\lambda_\varepsilon=0$. In expression (5) the term with $k=s=0$ corresponds to the TF model and, correspondingly, the sum (5) without this term, according to Eq. (2), determines the desired quantity $\delta N_{\rm sh}(\mu)$.

We note that even though the use of the TF potential is a more consistent procedure in the quasiclassical approximation, the relations (1)–(5) can be used to distinguish shell effects in any potential, simulating a self-consistent one, assuming that the normalization conditions hold for the term with $k=s=0$ in Eq. (5).

3. The points $\bar{\lambda}$ of stationary phase make the main contribution to the integral of the oscillatory function in Eq. (5). These points are determined from the relation

$$-\frac{\partial\nu_{\mu\lambda}}{\partial\lambda}\Big|_{\bar{\lambda}}=\frac{s}{k},\quad 0\leqslant\lambda\leqslant\lambda_\mu. \tag{6}$$

The function $\nu_{\mu\lambda}$ decreases monotonically, and for all potentials $U(r)$ that are finite at the origin the slope of the corresponding curve at $\lambda=0$ is the same,

$$-\frac{\partial\nu_{\mu\lambda}}{\partial\lambda}\Big|_0=-\frac{1}{2},$$

and the maximum value of the derivative obtains at $\lambda=\lambda_\mu$. This quantity

$$\frac{\partial\nu_{\mu\lambda}}{\partial\lambda}\Big|_{\lambda_\mu}\equiv-\nu'_\mu$$

depends strongly on the form of the potential. For an oscillator $\nu'_\mu=1/2$, for a ''square-well'' $\nu'_\mu=0$, and for the Woods–Saxon potential the value of ν'_μ varies with increasing N, vanishing in the limit of a very large number of atoms.

On this basis it follows that the relation (6) distinguishes in the sum over k the leading terms

$$k=(2+j)s, \quad -\frac{\partial \nu_{\mu\lambda}}{\partial\lambda}|_{\bar{\lambda}_j}=\frac{1}{2+j}, \tag{7}$$

$$j=0,1,\ldots j_{\max}, \quad j_{\max}=\left[\frac{1}{\nu'_\mu}-2\right].$$

The terms with $k=2s$ must be studied separately, since in this case the point of stationary phase is also the lower limit of integration. As a result, taking the terms $\{k=0,\ s\neq 0\}$ into account, we obtain

$$\delta N_{\rm sh}=\sum_{s=1}^{\infty}\frac{(-1)^s}{(\pi s)^2}\left\{\frac{\cos\,(2\pi s 2\nu_{\mu 0})}{\delta_\mu^{(0)}}-\lambda_\mu\left(2\nu'_\mu+\frac{1}{0.5-\nu'_\mu}\right)\cos\,(2\pi s\lambda_\mu)\right.$$
$$\left.-\sum_{j=1}^{j_{\max}}\frac{4\sqrt{s}\cdot j\cdot(-1)^{j\cdot s}}{(\delta_\mu^{(j)})^{3/2}(2+j)^{5/2}}\cos\left[2\pi s((2+j)\nu_{\mu\bar{\lambda}_j}+\bar{\lambda}_j)-\frac{\pi}{4}\right]\right\}. \tag{8}$$

Here

$$\delta_\mu^{(j)}\equiv\frac{\partial^2\nu_{\mu\lambda}}{\partial\lambda^2}|_{\bar{\lambda}_j}.$$

Substituting expression (8) into Eq. (1) and separating the terms which are of leading order in the quasiclassicity parameter using integration by parts gives a formula for the shell correction to the binding energy of electrons in a cluster in the quasiclassical approximation:

$$\delta E_{\rm sh}=\frac{1}{2}\sum_{s=1}^{\infty}\frac{(-1)^s}{(\pi s)^3}\left\{\frac{\sin\,(2\pi s 2\nu_{\mu 0})}{\delta_\mu^{(0)}(\partial 2\nu_{\mu 0}/\partial\mu)}-\frac{\lambda_\mu(2\nu'_\mu+(1/0.5-\nu'_\mu))\,\sin\,(2\pi s\lambda_\mu)}{(\partial\lambda_\mu/\partial\mu)}\right.$$
$$\left.-\sum_{j=1}^{j_{\max}}\frac{4\sqrt{s}\cdot j\cdot(-1)^{j\cdot s}}{(\delta_\mu^{(j)})^{3/2}(2+j)^{5/2}}\frac{\sin\,[2\pi s((2+j)\nu_{\mu\bar{\lambda}_j}+\bar{\lambda}_j)-\pi/4]}{\partial((2+j)\nu_{\mu\bar{\lambda}_j}+\bar{\lambda}_j)/\partial\mu}\right\}. \tag{9}$$

The terms in the sum over j in expression (9) are contributions from a set of levels — supershells, for which the corresponding combination of orbital and radial quantum numbers is quantized: $n_j=(2+j)n_r+l$, and the quantization at the Fermi energy is substantial. The proposed approach makes it possible to determine for any potential the period and amplitude of oscillations associated with each supershell and to estimate their relative role in the appearance of beats. The results of such an analysis for a ''square-well'' potential

$$U(r)=\begin{cases}-2\varepsilon_F, r\leqslant R\\ 0, r>R\end{cases}, \quad \mu=-\varepsilon_F,$$

are displayed in Fig. 1. We note that the total sum over j in Eq. (9) for $N>100$ agrees very well with the results of an exact calculation.[5] It is evident from the figure that the first period of the beats ($N^{1/3}\leqslant 7$) is determined by terms with $j=0,1,2$. The term with $j=3$ must be taken into account to produce the second period ($N^{1/3}\leqslant 13$). Adding a term

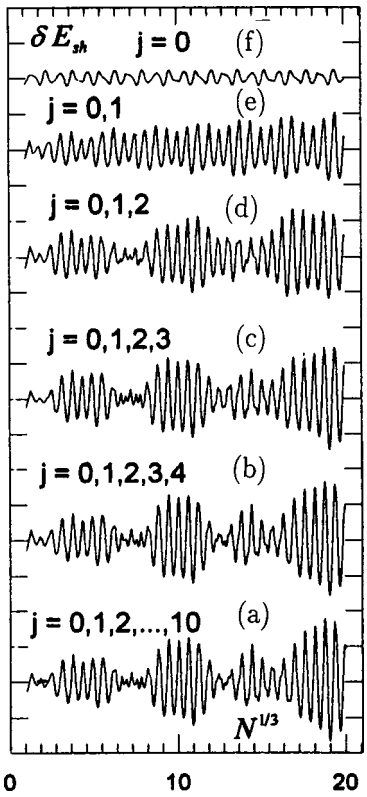

FIG. 1. a — Shell part $\delta E_{\rm sh}$ of the electron binding energy as a function of the number N of atoms in a cluster according to Eq. (9). b–e — Analysis of the contributions of various supershells. The unit of measurement is the Fermi energy ε_F.

with $j=4$ is sufficient to describe the behavior of $\delta E_{\rm sh}$ in the entire range under study. This means that the actual value of $j_{\max}$ is less than that determined from Eq. (7) and corresponds to actually filled states, for which

$$\nu_{\mu\bar{\lambda}_j} \geqslant \frac{1}{2}.$$

According to the theory developed in Ref. 6 for a spherical cavity, supershells with $K=2,3,4$ ($j=0,1,2$) correspond to classical ''billiard ball'' electron trajectories: a linear trajectory passing through the point $r=0$, ''triangular,'' and ''square.'' The supershells with $K=5$ and 6 obtained in our calculations are related with regular pentagons and hexagons.[8]

[1] W. A. de Heer and Rev, Rev. Mod. Phys. **65**, 612 (1993).
[2] M. Brack, Rev. Mod. Phys. **65**, 677 (1993).
[3] O. Genzken and M. Brack, Phys. Rev. Lett. **67**, 3286 (1991).
[4] H. Nishioka, K. Hansen, and B. R. Mottelson, Phys. Rev. B **42**, 9377 (1990).
[5] K. Clemenger, Phys. Rev. B **44**, 12991 (1991).
[6] R. Balian and C. Bloch, Ann. Phys. **69**, 76 (1971).

[7] S. Bjørnholm, in *Nuclear Physics Concepts in Atomic Cluster Physics* (Springer, New York, 1992) p. 26.
[8] E. Koch, Phys. Rev. B **58**, 2329 (1998).
[9] D. A. Kirzhnits, Yu. E. Lozovik, and G. V. Shpatakovskaya, Usp. Fiz. Nauk **117**, 3 (1975) [Sov. Phys. Usp. **18**, 649 (1975)].
[10] B. G. Englert, *Semiclassical Theory of Atoms*, Vol. 300 of Lecture Notes in Physics (Springer, New York, 1988).
[11] G. V. Shpatakovskaya, Teplofiz. Vys. Temp. **23**, 42 (1985).
[12] E. A. Kuzmenkov and G. V. Shpatakovskaya, Int. J. Thermophys. **13**, 315 (1992).
[13] V. Kresin, Phys. Rev. B **38**, 3741 (1988).
[14] M. Membrado and A. F. Pacheco, Phys. Rev. B **41**, 5643 (1990).

Translated by M. E. Alferieff

Submillimeter-wave Josephson spectroscopy

M. Tarasov,*) A. Shul'man, O. Polyanskiĭ, and A. Vystavkin
Institute of Radio Engineering and Electronics, Russian Academy of Sciences, 103907 Moscow, Russia

E. Kosarev
P. L. Kapitsa Institute of Physics Problems, Russian Academy of Sciences, 117973 Moscow, Russia

D. Golubev
P. N. Lebedev Physics Institute, Russian Academy of Sciences, 117924 Moscow, Russia

E. Stepantsov
Institute of Crystallography, Russian Academy of Sciences, 117333 Moscow, Russia

M. Darula and O. Harnack
Insitute of Thin Film and Ion Technology, Research Center, 52425 Jülich, Germany

Z. Ivanov
Chalmers Technical University, S41296 Göteborg, Sweden

(Submitted 6 July 1999)
Pis'ma Zh. Éksp. Teor. Fiz. **70**, No. 5, 338–343 (10 September 1999)

A Josephson high-temperature superconducting (HTSC) submillimeter-wave spectrometer is designed, built, and experimentally investigated. The integrated detection structure of the spectrometer includes a YBCO Josephson junction on a bicrystalline boundary, a double-slot or log-periodic antenna, and a low-inductance resistive shunt. The selective detector response and the response at an intermediate frequency of 1.4 GHz are measured under the action of a signal in the frequency range 350–1250 GHz. Three methods of spectroscopy are investigated using this setup: 1) a method of Hilbert spectroscopy with processing of the detector response is implemented; 2) it is found that for a wide Josephson line at intermediate frequency (IF) the response has the same form as the detector response, making it possible to obtain a spectrum and the width of the generation line from IF response measurements; 3) for a narrow Josephson line the IF response corresponds to the regime of conversion with self-pumping. A new method is proposed for calculating the emission spectrum. The method consists of simple shift, summation, and subtraction operations. The advantages of the method are simplicity, high sensitivity, and high resolution. © *1999 American Institute of Physics.* [S0021-3640(99)00517-4]

PACS numbers: 07.57.Pt, 85.25.Cp

Millimeter and submillimeter wave spectrometers based on high-temperature superconducting (HTSC) Josephson junctions can operate in the temperature range 4–77 K.

Josephson mixers can have a noise temperature two to three times lower than that of spectrometers using Schottky diodes.[1,2] The method of Hilbert spectroscopy,[3] employed for processing the selective detector response of a Josephson junction, has been widely used to the present day. Another possible method of spectroscopy with a Josephson junction could be to employ a mixer mode with an external pump or with self-pumping.

In the mixer with self-pumping, the input signal at frequency f_s is mixed with the characteristic Josephson oscillations. If the input signal is monochromatic, then the linewidth of the converted signal at the intermediate frequency (IF) will correspond to the Josephson line width Δf_J, which is a natural measure of the spectral resolution of such a spectrometer. Shunting of the junction with a low-inductance resistive shunt can be used to improve the resolution of such a spectral instrument. According to theoretical estimates, the minimal two-band noise temperature of a Josephson mixer with self-pumping[1,2] corresponds to the physical temperature T for $f<0.2f_c$ and decreases as $8(f/f_c)^2$ as the frequency increases above f_c. A low-inductance shunt improves the noise temperature of the mixer with an external heterodyne and the resolution of a mixer with self-pumping.

The integrated detecting structure included a YBaCuO Josephson junction, formed by a bicrystalline MgO or sapphire substrate, and a gold complementary log-periodic or double-slot antenna. An 80–100 nm thick YBaCuO film was deposited by laser ablation. Two-micron wide junctions at 4.2 K possessed a 10 Ω normal resistance and a 300 μA critical current. The current–voltage characteristics (IVCs) of the experimental junctions possessed a low excess-current fraction, a Fraunhofer dependence of the critical current on the magnetic field, and oscillatory dependences of the Shapiro steps and critical current on the microwave power. Either integrated shunts, deposited on one substrate with a junction, or loops consisting of 5 mm in diameter and 50 μm thick gold wire, welded by ultrasonic welding to the contact pads, were used for the shunting junctions. Such shunts had a resistance of less than 0.1 Ω at 4.2 K and did not shunt substantially at the intermediate frequency 1.4 GHz.

The substrate with the detecting structure was placed on a flat surface of an elongate hyperhemispherical MgO lens, placed on the cold plate of a helium cryostat with an optical window. Backward-wave tubes (BWTs) for the ranges 350–650 and 880–1250 GHz were used as signal sources. Radiation from cold (77 K) and warm (300 K) loads was used as the source of the wide-band signal. A polyethylene beam splitter was used to mix the wide-band signal with the BWT radiation. Black polyethylene and Fluorogold filters were used to eliminate any influence of IR overheating of the sample at the 77 K and 4 K steps. The IF signal was fed through a matching circuit to an amplifier, cooled to 4.2 K, with a cold circulator at the entrance.

The curves of the selective detector response and IF signal under the action of external radiation at frequencies up to 1250 GHz were measured (Fig. 1). It was found that the curves of the IF signal, just as the detector response, can be used to determine the width of the generation line and the frequency of the perturbing signal (Fig. 1b), since the maxima and minima of the detector response and the IF response coincide if the width of the Josephson line is greater than the intermediate frequency. The calculation of the signal spectrum from the modified detector response by the Hilbert transform method is known as Hilbert spectroscopy,[3] and the proposed IF response method can be regarded as a modification of the Hilbert method, making it possible to simplify the measurement

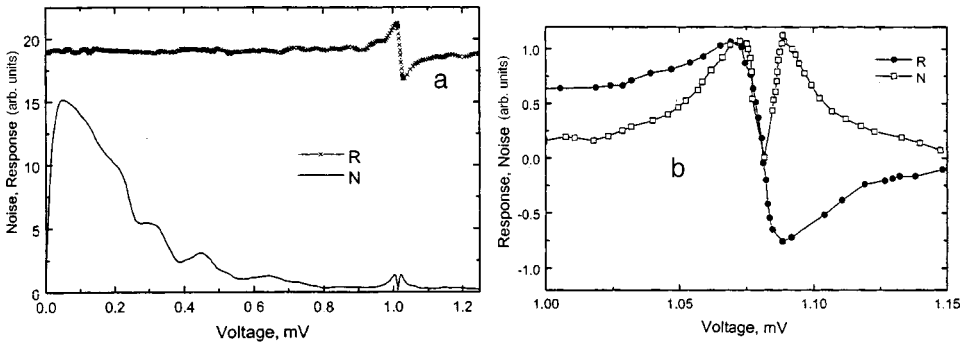

FIG. 1. a) Noise (*Np*,*Na*) and IVC (I), measured under the action of 0.5 THz irradiation (*Np*) and without irradiation (*Na*). b) Selective detector response *R* and noise *DN*, the latter after subtracting out the autonomous noise and extracting a square root. The generation linewidth is greater than the IF.

technique and to improve the sensitivity and frequency resolution. At 1000 GHz and temperature 4.2 K the generation linewidth was 34 GHz for a 20 Ω junction, 28 GHz for a 4 Ω junction, and 4.5 GHz for a junction with a 0.7 Ω resistive shunt. These values are six to eight times greater than the simple estimates from calculations based on the resistive model of a Josephson junction with thermal shunts as the main source of fluctuations $\Delta f[\mathrm{MHz}]=40(R_d^2/R_n)T[\mathrm{K}]$ (see Refs. 1 and 2).

A reconstructed spectrum, obtained by the Hilbert transform method from the detector response, with irradiation at 0.5 THz is presented in Fig. 2. The rf response curves measured for a wide intrinsic generation band ($\Delta f_J > f_{IF}$) have maxima and minima at the same values of the bias voltage as the detector response. For this case, the values of the generation linewidth and the signal frequency can be obtained just as in the case of a synchronous detector. If the IF is greater than the Josephson linewidth, $\Delta f_{IF} > f_J$, the positions of the maxima of the IF signal correspond to the sum and difference of the voltages at the signal frequency $V_s = f_s \Phi_0$ and at the IF $V_{IF} = f_{IF} \Phi_0$. Such a conversion regime has been investigated in detail in Ref. 4. This case can be easily modeled numerically using analytical relations. Figure 3 shows the computed dependences of the con-

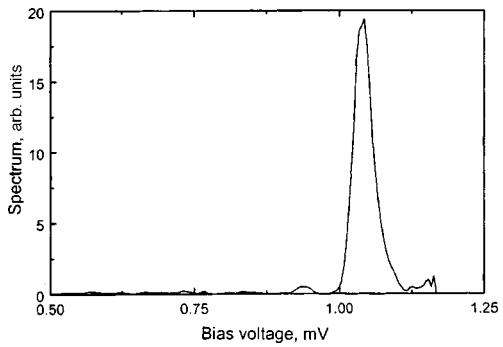

FIG. 2. Spectrum obtained from the detector response using a Hilbert transform.

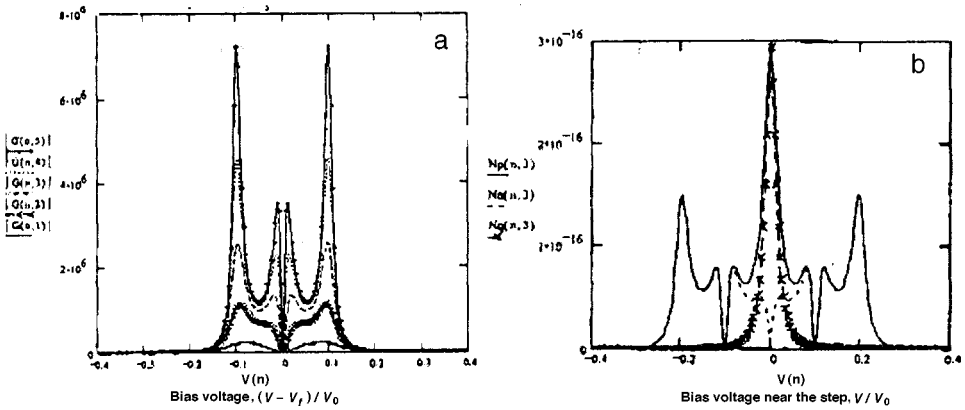

FIG. 3. a) Calculation of the conversion gain G near a Shapiro step. The maximum near the voltage step ($V=0$) corresponds the maximum of R_d, while the maxima located farther away correspond to a shift by the intermediate-frequency voltage $|V-V_f|=V_{IF}=0.1V_0$. b) Sum of Np and difference Nn of the shifted dependences and the reconstructed spectrum Nq.

version gain on the bias voltage for different values of the Q. Qualitatively, these dependences correspond to the measured values in Fig. 1.

We propose a simple numerical processing method to extract a spectrum from these dependences. The method includes subtraction of the autonomous value $Na(v)$ of the noise without the signal from the values $Np(v)$ obtained by feeding the signal, for the same values of the constant bias (see Fig. 4),

$$Ne(v)=Np(v)-Na(v). \tag{1}$$

Next, these dependences are shifted with respect to bias voltage by $+v_{if}$ and $-v_{if}$, where $v_{if}=f_{iv}\Phi_0$,

$$Ne(v+v_{if}) \quad \text{and} \quad Ne(v-v_{if}). \tag{2}$$

The sum and differences of these dependences are obtained:

$$Ns(v)=Ne(v+v_{if})+Ne(v-v_{if}), \tag{3}$$

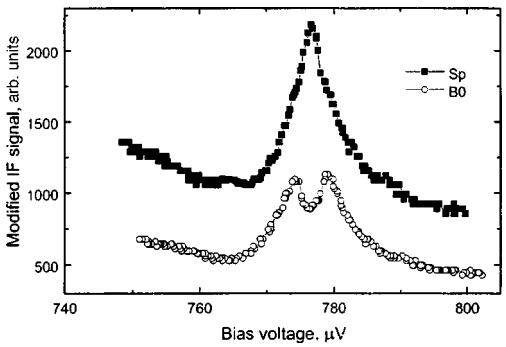

FIG. 4. Experimental curve of the output IF signal (squares) and the reconstructed spectrum (circles).

$$Nd(v)=Ne(v+v_{if})-Ne(v-v_{if}). \tag{4}$$

The desired spectrum is obtained from the last two functions as

$$S(v)=Ns(v)-|Nd(v)|. \tag{5}$$

Examples of such a calculation are presented in Fig. 3 for a model theoretical curve and in Fig. 4 for an experimental dependence.

The positions of the maxima of the detector response can be obtained from the analytical expression for the IVC of a Josephson junction near Shapiro steps in the presence of thermal noise of a normal resistance R_0. The blurring of the steps is characterized by the dimensionless parameter

$$\gamma=2ekT/\hbar I_{st}, \tag{6}$$

where I_{st} is the half-width of a step in the absence of noise. Exact analytical calculations are quite laborious, but simplified relations can be derived for practical estimates:

$$\Delta V\cong 1.92R_0\sqrt{2ekTI_{st}/h} \quad \text{for } \gamma\leqslant 1, \tag{7a}$$

$$\Delta V\cong 4\sqrt{3}kTR_0/h \quad \text{for } \gamma\geqslant 1, \tag{7b}$$

$$\Delta V=2f_{if}h/2e \quad \text{for} \quad I_{st}\cong 0. \tag{7c}$$

It is evident from these relations that when the Josephson linewidth is greater than the intermediate frequency, the positions of the maxima of the detector response and the IF response are the same. For the opposite case, the position of the detector response remains near the maximum of R_d, and the maxima of the IF response lie in the region of the side bands of the self-pumped mixer, i.e., at the voltages $V_{\max}=(f_J\pm f_{if})\Phi_0$. The sensitivity of these methods is determined, to a first approximation, by the sensitivity of the amplifiers. For a low-frequency detector response, the sensitivity is limited by noise with a $1/f$ spectrum and the amplifier noise can be estimated as $V_N=5$ nV/Hz$^{1/2}$. The noise temperature of the cooled amplifier at the IF can be less than 10 K. With a 0–10 dB conversion gain of the self-pumped mixer and a measured noise temperature of the order of $T_N\approx 1000$ K, and taking the sensitivity of the detector to be $\eta=10^6$ V/W,[5] the spectral density of the noise for detector and mixer spectrometers can be estimated as

$$S_{\text{det}}=V_N/\eta=5\times 10^{-9}/10^6=5\times 10^{-15}\ \text{W/Hz}^{1/2}, \tag{8}$$

$$S_{\text{spm}}=k\cdot T_N=1.4\times 10^{-23}\times 1000=1.4\times 10^{-20}\ \text{W/Hz}^{1/2}. \tag{9}$$

The frequency resolution of both methods corresponds to the Josephson linewidth, which can be greatly improved by using a low-inductance shunt. Such shunting something will not change the IF response much, but it will greatly decrease the selective detector signal; this indicates that the rf response method is preferable for improving the resolution and sensitivity of the spectrometer. Another advantage of the rf method is its insensitivity to the step size, making it possible to increase substantially the dynamic range of the apparatus.

In summary, a submillimeter-range HTSC Josephson spectrometer has been developed, built, and experimentally investigated. A new method of spectroscopy based on a self-pumped mixer mode was proposed and a method for extracting the spectrum of the experimental signal from the measured rf response was proposed. The spectroscopy

method proposed using a Josephson self-pumped mixer at a high intermediate frequency makes it possible to improve substantially the sensitivity, spectral resolution, and dynamic range of the Josephson spectrometer.

We thank the Russian Science and Technology Program ''Current Directions in Condensed-Matter Physics,'' the Russian Fund for Fundamental Research, the Ministry of Science of the Russian Federation, and the Swedish Royal Academy of Sciences for financial support.

*)e-mail: tarasov@hitech.cplire.ru

[1]K. K. Likharev and V. V. Migulin, Radiotekh. Élektron. **25**, 1 (1980).
[2]V. P. Zavaleev and K. K. Likharev, Radiotekh. Élektron. **23**, 1268 (1978).
[3]Yu. Ya. Divin, O. Yu. Polyanskiĭ, and A. Ya. Shul'man, Pis'ma Zh. Tekh. Fiz. **6**, 1056 (1980) [Sov. Tech. Phys. Lett. **6**, 454 (1980).
[4]V. P. D'yakov, K. K. Likharev and M. A. Tarasov, Radiotekh. Élektron. **25**, 1736 (1980).
[5]V. A. Il'in, K. Z. Fatykhov, and V. S. Étkin, Pis'ma Zh. Tekh. Fiz. **6,** 649 (1980) [Sov. Tech. Phys. Lett. **6**, 280 (1980)].

Translated by M. E. Alferieff

Low-frequency lattice dynamics in $Ba_{1-x}K_xBiO_3$ oxides according to ^{39}K NMR data

K. N. Mikhalev, S. V. Verkhovskiĭ, A. P. Gerashchenko, and Yu. V. Piskunov
Institute of Metal Physics, Ural Branch of the Russian Academy of Sciences, 620219 Ekaterinburg, Russia

A. Yu. Yakubovskiĭ
Kurchatov Institute Russian Science Center, 123182 Moscow, Russia

A. P. Rusakov
Moscow Institute of Steels and Alloys, 117026 Moscow, Russia

(Submitted 13 July 1999)
Pis'ma Zh. Éksp. Teor. Fiz. **70**, No. 5, 344–349 (10 September 1999)

The spin–lattice relaxation times T_1 in $Ba_{1-x}K_xBiO_3$ ($x=0.3$, 0.4, 0.5) were measured in the normal temperature range (20–300 K). A substantial contribution to the spin–lattice relaxation rate from dynamic local distortions of the crystal lattice near potassium atoms is found. The activation energy of this process increases with decreasing potassium concentration, and the frequency of lattice excitations decreases. The nature of the low-frequency lattice dynamics is discussed.

[S0021-3640(99)00617-9]

PACS numbers: 76.60.Es, 63.20.Kr, 74.25.Kc

The cubic perovskite $Ba_{1-x}K_xBiO_3$ exhibits the highest superconducting transition temperature ($T_C \sim 28$ K, $x \sim 0.4$) among oxides without copper.[1,2] A characteristic feature of this system is the absence of local magnetic moments and metal–oxygen planes, which largely determine the high superconducting transition temperatures T_C in copper oxides.

Indeed, it has been shown in a number of works[3,4] that the observed values of T_C can be explained on the basis of the Bardeen–Cooper–Schrieffer (BCS) theory in the strong-coupling approximation. However, in Refs. 3 and 4 the electron–phonon coupling constant was obtained using data from band calculations,[5] where the calculation is based on an ideal crystal lattice. Estimates of the electronic density of states from the specific heat were used as a criterion of correctness of the approximation employed. The variance of these data is very large.[6,7] An experimental work on the optical spectroscopy of this system appeared very recently.[8] The electron–phonon interaction constant in the normal temperature range was found to be much smaller ($\lambda=0.2$) than previously thought, which makes it impossible to the strong-coupling approximation to calculate T_C.

Data showing that the real structure of the system under study is substantially different from the ideal structure have recently appeared. In Ref. 9 the compound

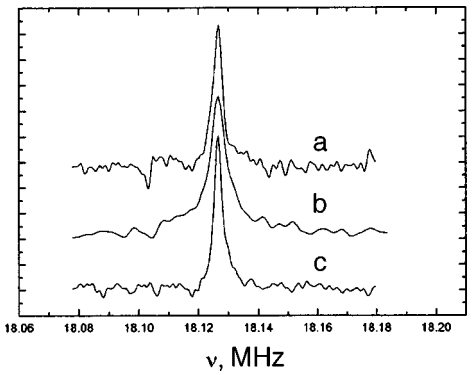

FIG. 1. ^{39}K NMR spectra of the oxide $Ba_{1-x}K_xBiO_3$ studied at $T=295$ K: a) $x=0.5$; b) $x=0.4$; c) $x=0.3$.

$Ba_{0.6}K_{0.4}BiO_3$ was investigated by EXAFS, a method sensitive to local lattice distortions. It was shown that in this compound a finite number of BiO_6 octahedra undergo anharmonic vibrations with frequencies much lower than the phonon frequencies.

Nuclear magnetic resonance is the most informative method for studying local static and dynamic structural distortions in solids. In a previous work[10] we showed, specifically, that the spin lattice relaxation rate of ^{137}Ba in $BaPb_xBi_{1-x}O_3$ at temperatures below 100 K shows exponential behavior, which was attributed to the thermal activation of the local motion of groups of BiO_6 octahedra, whose activation energy increases as the semiconductor composition is approached.

In the present letter we discuss the behavior of the spin–lattice relaxation rates of ^{39}K in $Ba_{1-x}K_xBiO_3$ in the normal temperature range. ^{39}K is an extremely convenient nucleus for use in NMR. Possessing spin $I=3/2$, it is sensitive to local disturbances of the charge distribution in the lattice. At the same time, the small quadrupole moment implies the existence of a narrow NMR line, as a result of which the relaxation times can be measured simply and reliably.

The ^{39}K NMR spectra of a series of $Ba_{1-x}K_xBiO_3$ samples were recorded in the temperature range 20–300 K on a pulsed NMR spectrometer with quadratic signal detection, using a $\pi/2-\tau-\pi-$ echo pulse sequence, followed by Fourier transformation of half of the echo. The spin–lattice relaxation time T_1 was measured using a saturating sequence.

The room-temperature ^{39}K NMR spectra in $Ba_{1-x}K_xBiO_3$ are displayed in Fig. 1. The spectrum consists of a single narrow line whose width at half-height is 3 kHz. The linewidth does not depend on the potassium concentration and increases very little with decreasing temperature. The line shift (position of the maximum) is zero and is independent of concentration and temperature.

The small line width at half-height for compositions with $x=0.4$ and 0.5 and for the composition with $x=0.3$ at $T>170$ K as well as the absence of quadrupole satellites can be explained by the cubic symmetry of the environment around potassium for these compositions and temperatures according to the phase diagram.[11] The concentration and temperature independence of the ^{39}K NMR line position can be understood by assuming

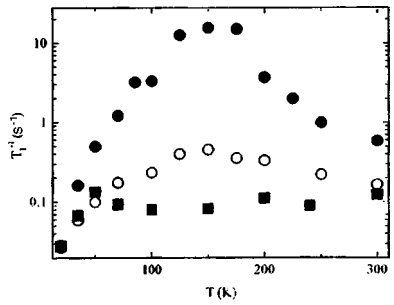

FIG. 2. Temperature dependence of the spin–lattice relaxation rate of ^{39}K in $Ba_{1-x}K_xBiO_3$. ● — $x=0.3$; ○ — $x=0.4$; ■ — $x=0.5$.

the *s* electrons of potassium do not participate in the formation of the conduction band, in agreement with band calculations, at least for the $Ba_{0.6}K_{0.4}BiO_3$ sample. However, it is known that the conductivity of the system $Ba_{1-x}K_xBiO_3$ depends strongly on the potassium concentration: for $x>0.4$ the conductivity is metallic, while for $x=0.3$ it corresponds to semiconductor behavior of the electric resistance. Thus, the shift was expected to depend on the concentration. At the same time, as follows from the phase diagram,[11] for the sample with $x=0.3$ a structural transition occurs at $T=170$ K from the cubic (high temperatures) into the orthorhombic phase. In this case, estimates show that two additional satellite lines, which correspond to a quadrupole frequency $\nu_Q=0.2-0.3$ MHz, and additional quadrupole broadening of the central transition line should appear in the ^{39}K NMR spectrum in the orthorhombic phase. This is not observed experimentally. It can be inferred that either the error in determining the temperature of the structural transition for this composition in constructing the phase diagram is large or the quadrupole interaction is averaged by fast local motion with frequencies higher than the characteristic NMR frequencies.

Figure 2 shows the temperature dependence of the spin–lattice relaxation rate T_1^{-1} for the three samples investigated. The dependences obtained are nonmonotonic, and a characteristic peak in the behavior of this quantity can be extracted for each curve. The amplitude of the peak increases substantially as *x* decreases. The temperature corresponding to the peak also increases. The similar anomaly in the behavior of the spin–lattice relaxation rate could be due to either structural changes in the sample or motion of the nucleus itself or the atoms in the nearest-neighbor environment. Since for compositions with $x=0.5$ and $x=0.4$, according to the phase diagram, the structure is cubic and does not change in the entire temperature range, it must be inferred that the observed maximum is due to the local motion of atoms in the lattice. We shall express the relaxation rate in the form of two basic contributions:

$$T_1^{-1}=T_{1e}^{-1}+T_{1Q}^{-1}. \tag{1}$$

Here T_{1e}^{-1} is the contribution due to the interaction of nuclear spins with the conduction electrons (Korringa contribution) and T_{1Q}^{-1} is the contribution due to the interaction of the quadrupole moment of potassium with the electric field gradient (EFG), modulated by motion in the lattice.

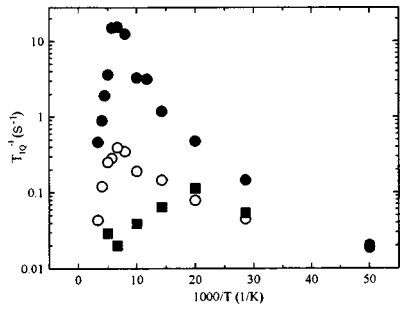

FIG. 3. The contribution due to motion in the lattice to the ^{39}K spin–lattice relaxation rate T_{1Q}^{-1} in $Ba_{1-x}K_xBiO_3$ versus the reciprocal temperature: ● — $x=0.3$; ○ — $x=0.4$; ■ — $x=0.5$.

For potassium, which has only an *s* electron in the outer shell, the Korringa contribution is proportional to the squared density of *s* states:

$$T_{1e}^{-1}=2h\gamma^2 k_B H_s^2 N_s^2(E_F)T, \tag{2}$$

where h is Planck's constant, k_B is Boltzman's constant, H_s is the hyperfine field induced at a potassium atom by the conduction-band electrons, $N_s(E_F)$ is the electronic density of states at the Fermi level, and T is the temperature. This contribution can be extracted, at least, for the composition $Ba_{0.5}K_{0.5}BiO_3$, which according to the phase diagram is close to a metal. Indeed, as one can see from Fig. 2, the Korringa contribution to the spin–lattice relaxation rate will predominate for this sample in the temperature ranges $T<20$ K and $T>100$ K. Taking a reasonable value for the hyperfine field, $H_s=5.8\times10^5$ Oe,[12] we estimate from Eq. (2) the electronic density of states at the Fermi level as $N_s^2(E_F)\sim0.2$ eV^{-1}. This value is at least an order of magnitude lower than the reasonable values of the density of states for this compound. This confirms the results of band calculations,[5] whence follows that the contribution of the *s* electrons of potassium to the total electronic density of states is close to zero. The smallness of this value and the fact that the relaxation rates for all experimental samples at $T=20$ K are essentially the same, suggests that the Korringa contribution is the same for all the samples investigated, and it can be subtracted from the experimental data.

Figure 3 shows the result of subtracting out the electronic contribution to the relaxation rate. It is evident that the maximum in the temperature dependence of the relaxation rate shifts into the high-temperature range as the potassium concentration x decreases, and at the same time the amplitude of the change in this quantity increases substantially. Let us assume that fluctuations of the electric field gradient at the location of the nucleus — probe (potassium) give rise to relaxation. We introduce the characteristic correlation time τ_c or the lifetime of a single lattice excitation. In its simplest form the expression for the relaxation rate of the quadrupole moment can be obtained by assuming an exponentially decaying correlation function of the lattice vibrations $G^{(q)}(t)=G^{(q)}(0)\exp(-t/\tau_c)$. Then, in the limit of rapid motion, for $\tau_c^{-1}\gg\omega_0$, where ω_0 is the resonance frequency, we can write[13]

$$T_{1Q}^{-1}=12\nu_Q^2\tau_c\,. \tag{3}$$

TABLE I.

Compound –	Lattice type ($T=295$ K)	Lattice parameter, Å	T_C, K –	E_A, K –
$Ba_{0.7}K_{0.3}BiO_3$	Cubic ($Pm3m$)	$a=4.300(4)$	–	1400
$Ba_{0.6}K_{0.4}BiO_3$	Cubic ($Pm3m$)	$a=4.283(4)$	29	580
$Ba_{0.5}K_{0.5}BiO_3$	Cubic ($Pm3m$)	$a=4.270(4)$	–	140

Here $\nu_Q=3e^2qQ/h2I(2I+1)$ is the quadrupole frequency, eq is the principal value of the EFG tensor, eQ is the quadrupole moment of the nucleus, and I is the spin nucleus.

We shall also assume an Arrhenius dependence of the correlation time on the temperature and the activation energy of lattice vibrations

$$\tau_c=\tau_0\ \exp(E_A/kT). \tag{4}$$

On the basis of the relations (3) and (4), the logarithm of the spin–lattice relaxation rate should be a linear function of the reciprocal of the temperature at high temperatures. Indeed, the plot presented in Fig. 3 confirms the correctness of the assumption (4) and makes it possible to estimate the activation energy of the lattice vibrations. This data are presented in Table I in temperature units.

Several types of motion, which could give rise to a similar modulation of the EFG, are possible in the crystal lattice of the system under study:

— motion of potassium atoms along the potassium (barium) sublattice;

— local motion in the oxygen sublattice, oxygen being the nearest-neighbor of potassium;

— dynamic local structural distortions of the type collective rotations of BiO_6 octahedra; and,

— motion of oxygen holes between nonequivalent BiO_6 octahedra with a different valence of bismuth.

Motion of potassium atoms appears to us to be least likely, since the potassium–oxygen bond is essentially ionic and quite rigid: None of the methods confirms potassium motion in this system (especially the existence of a potassium sublattice). The motion of oxygen atoms with characteristic frequencies comparable to NMR frequencies would give rise to narrowing of the ^{17}O NMR line and undoubtedly would lead to the appearance of an additional contribution to the ^{17}O relaxation rate, similar to that observed in the present work. However, this is not observed, at least for the composition $Ba_{0.6}K_{0.4}BiO_3$.[14]

The motion of oxygen holes would influence primarily the interaction of the nuclear angular momentum with the conduction electrons. As we have already discussed, this contribution to the spin–lattice relaxation rate is quite small.

Thus, we consider the moist likely choice to be modulation of the EFG at the potassium positions as a result of dynamic structural distortions of the lattice of the type collective rotations of groups of octahedra. Such distortions can give rise to incommensurate structural modulation with characteristic lengths $d<100$ Å , which is assumed in Ref. 11. Indeed, analysis of the four nearest coordination spheres of the bismuth environment[15] established the presence of local disorder in the form of rotation of hydrogen octahedra by an angle of $\sim 4-5°$ around the pseudocubic axes [110] and [111]. Such rotations could give rise to a fluctuating component of the EFG $e^2qQ/h\sim 0.1$ MHz, which is entirely sufficient for such behavior of the relaxation rate. This conjecture is also supported by analysis of the pair radial distribution function in neutron diffraction experiments,[16] indicating the dynamic character of the lattice distortions.

The most suitable microscopic model of such dynamic distortions has been proposed in Ref. 9. These are collective anharmonic rotations of nonequivalent BiO_6 octahedra, leading to vibrations of oxygen atoms in a double-well potential. In addition, the difference of the energies of the potential wells in model calculations (250 K) is comparable to the activation energies obtained (Table I).

In conclusion, we briefly summarize the results of this letter.

1. The nonmonotonic behavior of the spin–lattice relaxation rate of ^{39}K in $Ba_{1-x}K_xBiO_3$ as a function of temperature attests to the existence of local dynamic distortions of the lattice. Low-frequency collective rotations of oxygen octahedra are the most likely type of distortion. The characteristic frequency of these rotations decreases with the potassium concentration in this system.

2. The activation energy E_A of this local motion increases with decreasing potassium concentration in the system investigated.

3. The density of electronic *s* states of potassium at the Fermi level is at least an order of magnitude less than the value obtained from the electronic coefficient in the specific heat. This confirms the results of band calculations.

This work was performed as part of the State Program of the Russian Fund for Fundamental Research in Condensed-Matter Physics (Project No. 99-02-16974).

[1] R. J. Cava, B. Batlogg, J. J. Krajewski *et al.*, Nature (London) **332**, 814 (1988).
[2] D. G. Hinks, B. Dabrovskii, J. D. Jorgenson *et al.*, Nature (London) **333**, 836 (1988).
[3] M. Shirai, N. Suzuki, and K. Motizuki, J. Phys.: Condens. Matter **2**, 3553 (1990).
[4] O. Navarro, Physica C **265**, 73 (1996).
[5] L. F. Mattheiss and D. R. Hamann, Phys. Rev. Lett. **60**, 2681 (1988).
[6] B. Batlogg, R. J. Cava, L. W. Rup *et al.*, Phys. Rev. Lett. **61**, 1670 (1988).
[7] S. E. Stupp, M. E. Reeves, D. M. Ginsberg *et al.*, Phys. Rev. B **40**, 519 (1989).
[8] H. J. Kaufmann, O. V. Dolgov, and E. K. H. Salje, Phys. Rev. B **58**, 9479 (1998).
[9] A. P. Menushenkov, K. V. Klement'ev, P. V. Konarev *et al.*, JETP Lett. **67**, 1039 (1998).
[10] K. Kumagai, Yu. Piskunov, A. Yakubovskii *et al.*, Physica C **274**, 209 (1997).
[11] S. Pei, J. D. Jorgensen, Dabrowskii *et al.*, Phys. Rev. B **41**, 4126 (1990).
[12] G. C. Carter, L. H. Bennett, and D. J. Kahan, *Metallic Shifts in NMR* (Pergamon Press, 1977).
[13] A. Rigamonti, Adv. Phys. **33**, 115 (1984).
[14] L. Reven, J. Shore, Sh. Yang *et al.*, Phys. Rev. B **43**, 10466 (1991).
[15] Y. Yacoby, S. M. Heald, and E. A. Stern, Solid State Commun. **101**, 801 (1997).
[16] H. D. Rosenfeld and T. Egami, in *Lattice Effects in High-T_c Superconductors*, edited by Y. Baryam and T. Egami (World Scientific, Singapore, 1992), p. 105.

Translated by M. E. Alferieff

Magnetoresistance of lightly doped $TmBa_2Cu_3O_x$ crystals. Reorientation of the antiferromagnetic structure in a magnetic field

E. B. Amitin,*) A. G. Baĭkalov, A. G. Blinov, L. A. Boyarskiĭ, V. Ya. Dikovskiĭ, K. R. Zhdanov, M. Yu. Kameneva, L. P. Kozeeva, and A. P. Shelkovnikov

Institute of Inorganic Chemistry, Siberian Branch of the Russian Academy of Sciences, Novosibirsk State University, 630090 Novosibirsk, Russia

(Submitted 15 July 1999)
Pis'ma Zh. Éksp. Teor. Fiz. **70**, No. 5, 350–355 (10 September 1999)

The magnetoresistance of lightly doped $TmBa_2Cu_3O_x$ single crystals is investigated in the temperature range 4.2–300 K for magnetic fields up to 12 T. For the antiferromagnetic sample ($x=6.3$), when the current and field lie in the *ab* plane, the magnetoresistance is the sum of an anisotropic and a background component. The existence of the anisotropic component is attributed to the restructuring of the antiferromagnetic domain structure in a magnetic field. © *1999 American Institute of Physics.* [S0021-3640(99)00717-3]

PACS numbers: 72.20.My, 75.50.Ee, 75.60.Ch, 74.72.Jt, 74.25.Ha

The radical change in the properties of $RBa_2Cu_3O_x$ compounds from a normal antiferromagnetic metal to a superconductor in a narrow range of oxygen concentrations $6.35<x<6.4$ is still one of the most intriguing characteristics of lightly doped cuprate systems. It is known from neutron diffraction analysis[1,2] that $YBa_2Cu_3O_x$ in the antiferromagnetic phase possesses a collinear spin structure with spins directed parallel to the [100] or [010] axes. Because of the equivalence of these directions in the tetragonal phase, the volume of the sample is partitioned into 90-degree antiferromagnetic domains. A recent neutron diffraction study[2] of the system $YBa_2Cu_3O_{6.3}$ presented proof of the existence of antiferromagnetic domain structure (ADS) and a rearrangement of this structure in a magnetic field. According to Ref. 2, a magnetic field in the *ab* plane tends to reorient the spin axes of different domains into a position perpendicular to the field. This result agrees with a theoretical analysis[3] predicting a transition of the magnetic structure of YBCO into a spin-flop phase, if a field higher than a certain value is applied in the directions of the spins. For ordinary antiferromagnetic metals, it is known (see, for example, Ref. 4) that the restructuring of the ADS strongly affects the transport properties, specifically, the magnetoresistance (MR). In a recent investigation[5] of the MR of YBaCuO antiferromagnetic single crystals, hysteresis phenomena were observed at low temperatures. The results of this work, from our standpoint, could be interpreted on the basis of a spin-flop transition. The present letter is devoted to a study of the effect of the reorientation of the magnetic structure on the MR and the resistivity of the system $TmBa_2Cu_3O_{6.3}$ (Ref. 6).

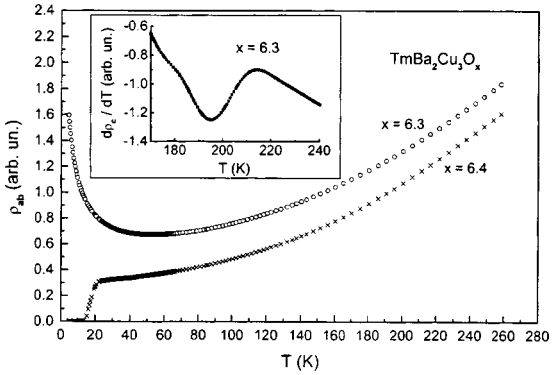

FIG. 1. Temperature dependences of the *ab* resistivity of $TmBa_2Cu_3O_x$ single crystals: ○ — sample No. 1 ($x=6.3$); × — sample No. 2 ($x=6.4$). Inset: Derivative of the resistance along the *c* axis of sample No. 3 ($x=6.3$) near the Néel point.

Experimental procedure and results

$TmBa_2Cu_3O_x$ single crystals were grown from a fluxed melt in alundum crucibles. Analysis of samples from a given batch showed that their aluminum content does not exceed 1%.[7] A $1.5\times0.2\times0.03$ mm (the smallest dimension is along the *c* axis) single-crystal wafer with oxygen content $x=6.3$ served as the object of investigation. Simultaneously with the main sample (No. 1), samples No. 2 ($x=6.4$, $1.5\times0.2\times0.03$ mm) and No. 3 ($x=6.3$, $0.5\times0.5\times1.0$ mm), cut out from the same batch, were also investigated. The working current lay in the *ab* plane in samples Nos. 1 and 2, and along the *c* axis in sample No. 3. Samples Nos. 1 and 3 were annealed together in order to obtain the same oxygen content. The samples were mounted on a turntable in such a way that the magnetic field always lay in the *ab* plane for samples Nos. 1 and 2 and in a plane normal to *ab* for sample No. 3. Fields up to 12 T were produced by an Oxford Instruments superconducting solenoid. The temperature was measured with a TSU-2 resistance thermometer, calibrated in a magnetic field.

Figure 1 shows the temperature dependences of the resistivity for samples Nos. 1 and 2. It is evident that the curves $\rho_{ab}(T)$ for oxygen concentrations $x=6.3$ and $x=6.4$ differ radically at low temperatures, where a superconducting transition ($T_c\approx15$ K) occurs in sample No. 2. For sample No. 1, the resistivity increases rapidly with decreasing temperature, which could indicate a nonmetallic ground state. The Néel temperature for the oxygen concentration $x=6.3$ (samples Nos. 1 and 3) is $T_N\approx195$ K. At this temperature a characteristic anomaly of the derivative of the *c* resistivity is observed (see inset in Fig. 1). It is noteworthy that no features near the Néel point are seen in the dependence $\rho_{ab}(T)$ for sample No. 1. This fact was indicated previously in Ref. 7.

The typical field dependences of the MR of No. 1 are shown in Figs. 2a–c. The plots are given for two orientations (relative to the current) of the magnetic field: $H\|I$ and $H\perp I$. Before each curve was obtained, the sample was heated to temperature 240 K, above T_N, to erase the magnetic past history, since pronounced hysteresis phenomena were present. In sample No. 1 the hysteresis was evidently due to the presence of mag-

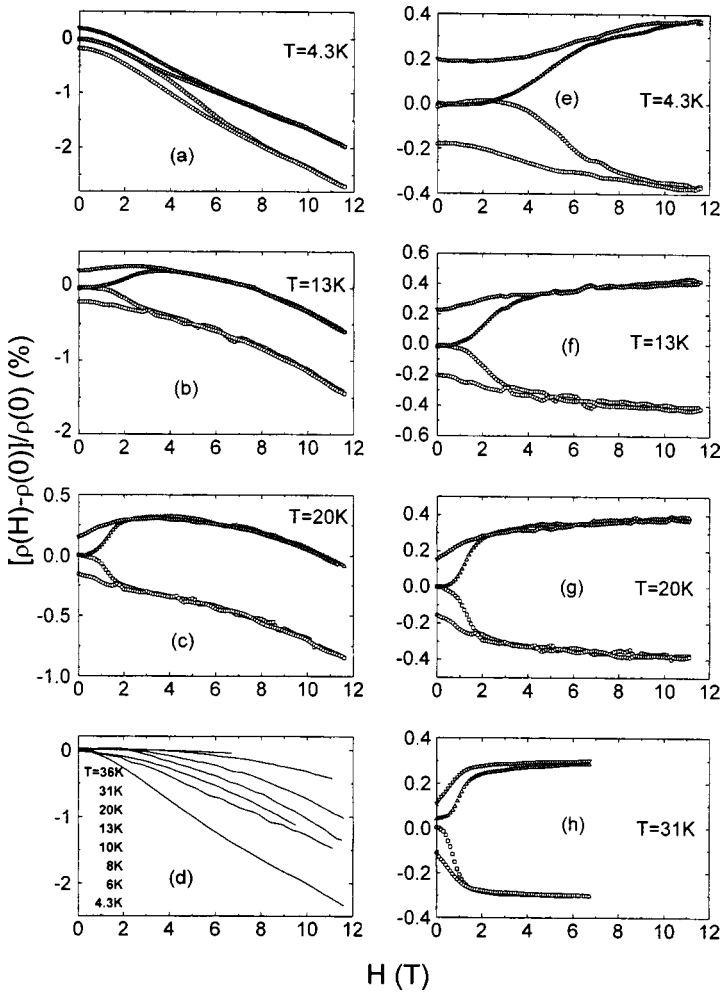

FIG. 2. Separation of the components of the magnetoresistance: a, b, c — typical field dependences of the MR in the *ab* plane of a $TmBa_2Cu_3O_{6.3}$ single crystal (sample No. 1) at low temperatures. The top and bottom parts of the hysteresis curves refer to the geometries $H \perp c$ and $H \perp I$, respectively; d — field dependences of the background MR at different temperatures; e–h — examples of the field dependences of the anisotropic component of the MR.

netic ordering, while no hysteresis was observed in the ''nonmagnetic '' sample No. 2. For the two chosen directions of the field, the hysteresis differed in sign: The difference of the curves $\rho(H)$ obtained with increasing and decreasing field was negative for $H \perp I$ and positive for $H \| I$. These differences were identical in absolute magnitude for these directions within the limits of experimental accuracy. This observation made it possible to divide the magnetoresistance into two components: an anisotropic component exhibiting hysteresis

$$\left(\frac{\Delta\rho}{\rho_0}\right)_a = \pm\frac{(\rho(H^{\perp}) - \rho(H^{\|})}{2\rho(0)}$$

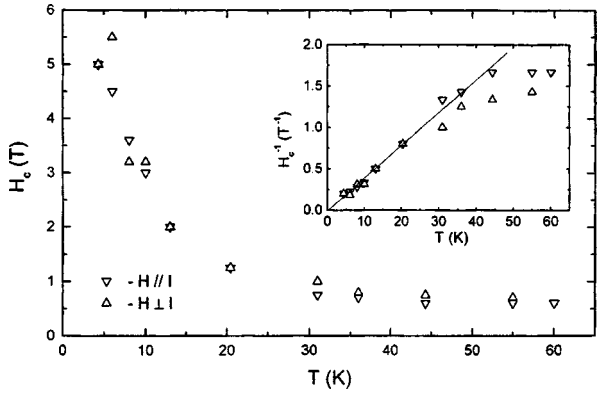

FIG. 3. Threshold field H_c versus the temperature, as determined from analysis of the field dependences of the irreversible magnetoresistivity. The symbols Δ and ∇ refer to the data corresponding to the geometries $H\perp I$ and $H\|I$, respectively. The values of H_c were determined from the extremum of the derivative $d\rho/dH$ on the curve obtained with the first increase in the field. Inset: Reciprocal of the threshold field versus the temperature.

and a hysteresis-free, background component

$$\left(\frac{\Delta\rho}{\rho_0}\right)_b = \frac{(\rho(H^{\perp}) + \rho(H^{\|}) - 2\rho(0))}{2\rho(0)}.$$

In these expressions $\rho(H^{\perp})$ and $\rho(H^{\|})$ are the curves obtained with increasing and decreasing field, while $\rho(0)$ is the initial (before application of the magnetic field) resistivity of the sample.

The behavior of the anisotropic component of the MR of sample No. 1 at various temperatures is displayed in Figs. 2e–g. On the basis of the form of the dependences $(\Delta\rho/\rho_0)_a(H)$, it can be conjectured that they describe a transition between two states occurring near a certain threshold field H_c. On the basis of the neutron data,[2] it is natural to assume that the sample in weak fields ($H<H_c$) is in a multidomain state, while in strong fields ($H\gg H_c$) the sample is a single-domain state with spin orientation perpendicular to the field (spin-flop phase). The quantity H_c was found from the extremum of the derivatives $d\rho/dH$ on the curve $\rho(H)$, obtained with the first (after erasure of the magnetic past history) increase of the field. The threshold field determined in this manner had close values for magnetic field directions $H\|I$ and $H\perp I$. Figure 3 shows the variation of H_c with temperature. It is evident that at low temperatures the threshold field decreases according to a law close to $H_c \sim T^{-1}$, while at high temperatures it stabilizes near $H_c \sim 0.7$ T. As temperature increases, the character of the hysteresis of the anisotropic MR also changes. According to Fig. 2, up to temperature 13 K the hysteresis at $H=0$ remains approximately constant, equal to $0.2\pm0.03\%$. A regular decrease of the hysteresis commences at higher temperatures, possibly because of a partial restoration of ADS. Similar behavior is characteristic for the anisotropic MR obtained in fields $H\gg H_c$, where $(\Delta\rho/\rho_0)_a$ tends to saturate. The difference is that in the single-domain region ($T \leqslant 13$ K) $(\Delta\rho/\rho_0)_a|_{H\gg H_c} \approx (0.4\pm0.03)\%$, which is two times greater than $(\Delta\rho/\rho_0)_a|_{H=0}$.

The background component of the MR was negative for the low-temperature region and positive for the high-temperature region. Its field dependence was close to quadratic

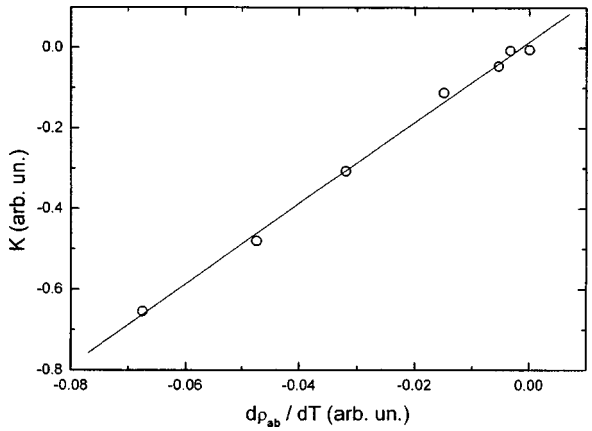

FIG. 4. Correlation of the background magnetoresistance coefficient K and the derivative $d\rho/dT$ of the resistivity for sample No. 1 in the temperature range 8–53 K.

$(\Delta\rho/\rho_0)_b \sim KH^2$, in agreement with the results of Ref. 5. The nonmonotonic behavior of the coefficient K as a function of the sign near 55 K qualitatively corresponds to the temperature behavior of the derivative of the resistivity of sample No. 1. Figure 4 compares quantitatively $K(T)$ and $d\rho/dT(T)$, whence it can be concluded that the variation of the quantities is similar at low temperatures.

Discussion

In summary, the *ab*-plane magnetoresistance of a magnetically ordered $TmBa_2Cu_3O_{6.3}$ crystal includes background and anisotropic components. The latter seems to reflect the restructuring of the ADS in a magnetic field, specifically, reorientation of the spin planes of various domains into a single-domain state corresponding to the spin-flop phase. In this case the threshold field for spin reorientation is determined as $H_c = \sqrt{2H_A \cdot H_E}$, where H_A and H_E are the anisotropy and exchange fields, respectively. In the temperature range $T \ll T_N$ of interest to us, the change in H_c reflects the temperature behavior of the anisotropy field, which turns out to be close to $H_a \propto T^{-2}$.

The existence of hysteresis in the anisotropic MR indicates complete or partial irreversibility of the restructuring of the ADS. The quantity $(\Delta\rho/\rho_0)_a|_{H=0}$ can serve as a measure of the irreversibility. A similar change in $(\Delta\rho/\rho_0)_a|_{H=0}$ and $(\Delta\rho/\rho_0)_a|_{H \gg H_c}$ with temperature could indicate that they have the same origin. We believe that both quantities characterize the anisotropy of the magnetic part of the *ab* resistance of the system $TmBa_2Cu_3O_x$. The fact that in a single-domain state the anisotropic MR at $H=0$ is half that at $H \gg H_c$ can be explained by rotation of the spins toward the nearest easy axis (edge of a tetragonal cell) after the field is switched on.

In principle, a change in the resistivity of a sample with restructuring of the ADS should include, aside from an anisotropic contribution associated with the reorientation of the spin structure, a contribution due to the vanishing or decrease of scattering by the domain walls. Thus, in Ref. 4, where the reorientation of the antiferromagnetic structure of europium in a magnetic field was studied, the domain contribution reached 60% of the anisotropic irreversible magnetoresistance. It follows from Fig. 2 that the irreversible

magnetoresistance of TmBaCuO does not contain substantial domain scattering. In the opposite case, the positive and negative irreversible contributions could not be symmetric for virtually all temperatures in the range of single-domain structure ($T \leqslant 13$ K).

The small anisotropic MR (0.2–0.4%) due to the reorientation of the spin structure in the temperature range $T < 20$ K is interesting. For europium in the single-domain state the similar quantity reached 8%.[4] Estimates show that this difference can be explained by the smallness of the spin scattering in TmBaCuO, due to the low spin of the Cu^{2+} ion. Indeed, the scale of the single-electron spin scattering is determined by the product $S(S+1)$, where S is the spin of a magnetic ion. Assuming that the spins of Cu^{2+} ($S = 1/2$) ions participate in the scattering, we obtain a contribution due to spin scattering that is 21 times smaller than in europium, whose spin $S = 7/2$, in agreement with experiment. In the present letter we do not discuss the effects due to strong electronic correlation, which are characteristic for cuprate compounds. The question of the influence of these effects on the restructuring of the ADS and electron–spin scattering processes remains open. An alternative explanation of anisotropic MR could be an influence of the magnetic structure on the carrier spectrum, i.e., a superband splitting effect. For TmBaCuO this effect is complicated, since the magnetic periodicity, which is twice the crystal periodicity, occurs along both edges of a tetragonal cell. The anisotropy which we observe could be the difference between the superband effects for mutually perpendicular directions in a CuO_2 layer.

The main features of the background component — independence from the orientation of the magnetic field and proportionality to the derivative of the resistance — have not yet been completely explained. As a possible reason for the appearance of an isotropic negative magnetoresistance, we are considering a change in the conditions of carrier localization in a magnetic field.

We thank I. N. Kuropyatnik for assistance in certifying the samples. This work is supported by the State program ''High-Temperature Superconductivity'' (Grant No. 98-009), the program ''Universities of Russia'' (Grant No. 1785), and the Federal Target Program ''Integration'' (Grant No. 274).

*)e-mail: amitin@casper.che.nsk.su

[1] J. M. Tranquada, D. E. Cox, W. Kunnman *et al.*, Phys. Rev. Lett. **60**, 156 (1988).
[2] P. Burlet, J. Y. Henry, and L. P. Regnault, Physica C **296**, 205 (1998).
[3] V. G. Bar'yakhtar, V. M. Loktev, and D. A. Yablonskiĭ, Sverkhprovodimost' (KIAE) **2**, 32 (1989) [Superconductivity **2**, 28 (1989)].
[4] L. A. Boyarskiĭ and V. Ya. Dikovskiĭ, Fiz. Nizk. Temp. **2**, 1297 (1976) [Sov. J. Low Temp. Phys. **2**, 632 (1976)].
[5] Y. Ando, A. N. Lavrov, and K. Segawa, http://xxx.lanl.gov/abs/cond-mat/9905071.
[6] L. S. Fritz and N. S. Dixon, Hyperfine Interact. **72**, Iss. 1–3, 191 (1992).
[7] A. N. Lavrov and L. P. Kozeeva, Physica C **248**, 365 (1995).

Translated by M. E. Alferieff

Observation of a dipole contribution to the magnetoresonant soft mode in Fe_3BO_6

V. D. Buchel'nikov
Chelyabinsk State University, 454021 Chelyabinsk, Russia

N. K. Dan'shin and Yu. I. Nepochatykh
Donetsk Physicotechnical Institute, Ukrainian National Academy of Sciences, 340114 Donetsk, Ukraine

V. G. Shavrov*)
Institute of Radio Engineering and Electronics, Russian Academy of Sciences, 103907 Moscow, Russia

(Submitted 3 August 1999)
Pis'ma Zh. Éksp. Teor. Fiz. **70**, No. 5, 356–359 (10 September 1999)

A jump in the frequency of the quasiferromagnetic soft mode in Fe_3BO_6 at the point of the spontaneous orientational phase transitions $\Gamma_2-\Gamma_4$ is observed experimentally. It is shown theoretically that this jump can be explained by the contribution of the dipole interaction to the expression for the quasiferromagnetic soft mode. © *1999 American Institute of Physics.* [S0021-3640(99)00817-8]

PACS numbers: 76.50.+g, 75.30.Kz

At temperatures $T<T_N=508$K the orthorhombic crystal Fe_3BO_6 undergoes ordering into an antiferromagnetic structure with weak ferromagnetism. Spontaneous reorientation of the ferromagnetism **F** and antiferromagnetism **G** vectors in the *xz* (*ac*) plane, $\Gamma_2(F_xG_z)\leftrightarrow\Gamma_4(G_xF_z)$, occurs in this material by a first-order orientational phase transition (OPT-1) at $T=T_{SR}=415$ K. In most compounds of this class (for example, in rare-earth orthoferrites) this same reorientation occurs continuously by two second-order orientational phase transitions (OPT-2): $\Gamma_2(F_xG_z)\leftrightarrow\Gamma_{24}(F_{xz}G_{xz})$ and $\Gamma_{24}(F_{xz}G_{xz})\leftrightarrow\Gamma_4(G_xF_z)$, i.e., via the canted phase $\Gamma_{24}(F_{xz}G_{xz})$.

A characteristic feature of the OPT-2 is that the resonance frequencies of the quasiferromagnetic soft mode σ in the phases on the two sides of the transition are the same at the transition point. By contrast, a characteristic property for OPT-1 is the occurrence of a jump in frequency at the transition point, i.e., the appearance of a frequency gap in the magnetoresonance spectrum of the σ mode. This effect is always observed in the field dependences of the resonance frequencies in the simplest magnetically ordered crystals, for example, at the point of the ''spin-flop'' transition in two-sublattice easy-axis antiferromagnets[1,2] or at metamagnetic transitions.[3] However, in complicated multisublattice magnets, especially in the presence of several magnetic subsystems consisting of ions of different kinds (which happens in rare-earth orthoferrites), the frequency jump at the point of the OPT-1 is not at all necessary. In such magnets the situation where the indicated jump does not occur at the OPT-1 point is not unique. For example, a jump in

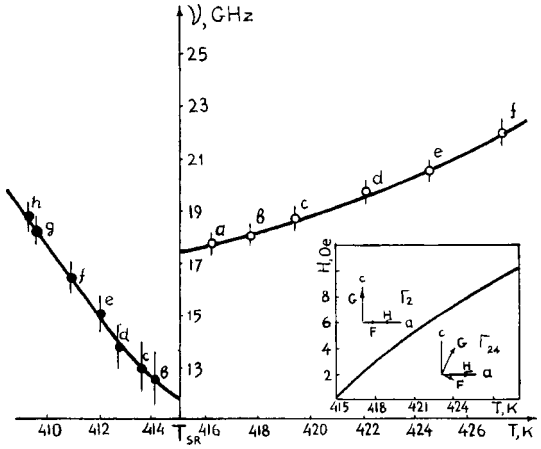

FIG. 1. Temperature dependences of the energy gaps in Fe_3BO_6 at the points of completion of the field-induced spin reorientation $\Gamma_{24}-\Gamma_4$ with $\mathbf{H}\|\mathbf{c}$ (●) and $\Gamma_{24}-\Gamma_2$ with $\mathbf{H}\|\mathbf{a}$ (○). Each point in the temperature dependences of the gaps corresponds to the following values of the field H (Oe): a — 1.25, b — 2.5, c — 4, d — 6, e — 8, f — 10, g — 12, h — 12.5. Inset: Fragment of the $H-T$ phase diagram of Fe_3BO_6 with $\mathbf{H}\|\mathbf{a}$ and the structure of the transition $\Gamma_{24}-\Gamma_2$ occurring with this orientation of the field.

the AFMR frequency is not observed at a Morin-type OPT-1 in $DyFeO_3$ (Ref. 4), while in $HoFeO_3$ (Ref. 5) it is clearly observed in the process of a complex spontaneous reorientation $\Gamma_2\rightarrow\Gamma_4$. Everything depends on the particular ratio of the anisotropy constants, which can make this effect very weak or, conversely, strong. The latter assertion also applies to the compound Fe_3BO_6, which is isomorphic to rare-earth orthoferrites.

In Ref. 6 it was concluded on the basis of a theory specially developed for Fe_3BO_6 that in this magnet the frequency jump and gap in the spectrum of the magnetoresonant soft mode should be absent at the point of the spontaneous reorientation $\Gamma_2-\Gamma_4$. These calculations took into account the dynamics of the spin subsystem only. The conclusion that a frequency jump and a gap are absent followed from the corresponding ratio of the magnetic anisotropy constants at the OPT-1 point. Such a conclusion is completely justified in the spin-wave approximation.

To check the results of Ref. 6, in view of the expected smallness of the effect, we used a highly sensitive modulation technique[7] in which the resonance absorption signals were recorded by scanning the temperature with the modulated magnetic field held fixed.

The experimental temperature dependences of the energy gaps — the minimum frequencies of the σ mode on the lines of the transitions induced by the magnetic field — are presented in Fig. 1. It is evident that extrapolating them to the point of the spontaneous OPT-1 ($H=0$, $T=T_{SR}$) from the sides of temperatures above and below T_{SR} gives nonzero and different values of the gaps at this point — with frequencies $\nu_1=11.8\pm1.5$ GHz and $\nu_2=17.5\pm1$ GHz, respectively. Unfortunately, the accuracy of the experiment in the limit $H\rightarrow0$ does not make it possible to identify these gaps with specific phases. However, as follows from the theoretical formulas presented below for the gaps at the point of the spontaneous OPT and from independent experiments[8–10] determining the Dzyaloshinskiĭ constants in Fe_3BO_6, the first frequency should corre-

spond to a gap in the Γ_4 phase and the second frequency to a gap in the Γ_2 phase.

Modern ideas about the mechanisms leading to the formation of energy gaps at the points of orientational transitions had to be used to explain the experimental observation of a large gap and a jump in the frequencies from the sides of the adjoining phases at the point of the spontaneous OPT-1, which were unexpected from the standpoint of the theory.[6] These ideas are based on taking the dynamic interaction of the spin subsystem with other vibrational subsystems of a magnet into account to the fullest extent possible.[11]

In Ref. 6 and in works cited therein, the effect of the magnetoelastic and dipole interactions on the spin-wave spectrum was neglected, although, as is well known,[11–14] the effect of these interactions on the spin-wave spectrum could become the governing influence near phase transitions. This assertion holds for OPT-1 and OPT-2.

In Ref. 12, the quasispin-wave spectra of rare-earth orthoferrites near a spontaneous OPT-1 were calculated taking into account the dipole and magnetoelastic interactions. In this work, expressions for the vibrational frequencies of the spin subsystem were obtained in the magnetostatic approximation. In Ref. 11 it was noted that the complete Maxwell's equations, and not the equations of magnetostatics, must be used to calculate the vibrational spectrum of the magnetic subsystem.

In the present work the vibrational spectrum of the spin subsystem was calculated using the methods developed in Refs. 11 and 12. For generality, we present here the computational results for the frequency of the magnetoresonant quasiferromagnetic soft mode σ for spontaneous and for magnetic-field induced OPTs.

The activations of the σ mode in the phases Γ_4 and Γ_2 have, respectively, the forms

$$\nu_{01}^2(g/2\pi)^2[-H_E(K_1+2K_2)/M_0+H_E(H_{me5}+H_{dip1})+H(H+H_{D1})], \tag{1}$$

$$\nu_{02}^2=(g/2\pi)^2[H_EK_1/M_0+H_E(H_{me5}+H_{dip2})+H(H+H_{D2})]. \tag{2}$$

Here H_E, H_{me5}, $H_{D1,2}$, and $H_{dip1,2}$ are, respectively, the homogeneous exchange field, the magnetostriction field, the Dzyaloshinskiĭ field, and the dipole interaction field, $K_{1,2}$ are the second- and fourth-order effective anisotropy constants (see Refs. 11 and 12), g is the gyromagnetic ratio, and M_0 is the saturation magnetization of the sublattices. The fields $H_{D1,2}$ and $H_{dip1,2}$ can be expressed as

$$H_{D1,2}=(3d_{3,1}-2d_{1,3})/M_0, \quad H_{dip1,2}=16\pi(d_{3,1}/H_E)^2/M_0, \tag{3}$$

where $d_{1,3}$ are the antisymmetric exchange constants (Dzyaloshinskiĭ constants).

Let us compare the theoretically derived formulas (1) and (2) for the resonance frequencies with the experimental results presented in the present work and in Ref. 7.

The point of the spontaneous OPT-1 $\Gamma_2-\Gamma_4$ is determined by the condition $K_1+K_2=0$ (a first-order phase transition is possible only for $K_2<0$).[11,12] Hence it follows that when the magnetoelastic and dipole interactions are neglected ($H_{me5}=0$ and $H_{dip}=0$) the activations in the resonant spectrum of the σ mode on the Γ_2 phase side and on the Γ_4 phase side are the same at the point of the spontaneous transition ($H=0$):

$$\nu_{01}^2=\nu_{02}^2=(g/2\pi)^2(-H_EK_2/M_0). \tag{4}$$

Therefore there will be no frequency jump at the phase transition point in this case. This was found in Ref. 6. In reality, however, as follows from the exact formulas (1) and (2), such a jump does exist. In zero magnetic field it is determined by the dipole contribution and it is give by

$$\Delta\nu^2=\nu_{02}^2-\nu_{01}^2=(g/2\pi)^2H_E(H_{dip2}-H_{dip1}). \quad (5)$$

We shall now estimate the numerical value of the frequency jump at the point of the spontaneous phase transition. For this, we employ the following values of the constants appearing in formulas (1) and (2): $H_E\approx5\times10^6$ Oe, $M_0\approx10^3$ G, $g\approx2\times10^7$ Hz/Oe, $d_1/M_0\approx14\times10^3$ Oe, $d_3/M_0\approx1\times10^4$ Oe.[6,8–10,12] Then we obtain for the numerical value of the frequency jump at the point of the spontaneous OPT $\Delta\nu\approx3$ GHz. This value agrees well with the experimental value $\Delta\nu\approx5.7$ GHz (see Fig. 1).

In summary, an effect that does not follow from the conventional description of the dynamics of ordered magnets near an OPT, i.e., neglecting the interaction of the spin subsystem with other vibrational subsystems, was observed in Fe_3BO_6. In this case this effect is due to the influence of the interaction of spin and electromagnetic waves on the magnetoresonance spectrum. It has not been ruled out that the previously observed frequency jump at the point of the spontaneous OPT-1 in $HoFeO_3$ (Ref. 5) likewise incorporates the corresponding dipole contribution. In principle this conjecture can be made with respect to any OPT-1, if the experimentally observed frequency jump at this point does not agree with the value computed taking account of only the dynamics of the spin subsystem.

It should also be noted that the comparative analysis, performed above, of the theory and experiment with respect to the role of spin dynamics in the formation of an energy gap and frequency jump took account of only the precession motion of the magnetization. When its longitudinal oscillations are taken into account, a gap of relaxational origin will also appear additively in expressions (1) and (2) for the quasispin-wave frequencies. This gap can make a large contribution to the total energy gap at high temperatures and (or) in strong magnetic fields.[10] In principle, if this gap is anisotropic in character, it could also contribute to the frequency jump at a spontaneous OPT-1. Just as the dipole contribution, the relaxational contribution due to interaction of precessional and relaxational oscillations to the energy gap could give rise to the discrepancy in the values of the gaps at the OPT points calculated for the case $H=0$ and obtained by extrapolating the experimental spectrum to $H=0$ from large values of the magnetic field, as was observed in the experiments of Ref. 7.

*)e-mail: shavrov@mail.cplire.ru

[1] V. V. Eremenko, A. V. Klochko, and V. M. Naumenko, JETP Lett. **35**, 591 (1982).
[2] V. G. Bar'yakhtar, A. P. Bogdanov, V. A. Popov, and A. P. Yablonskiĭ, JETP Lett. **41**, 367 (1985).
[3] N. K. Dan'shin, N. M. Kovtun, and M. A. Sdvizhkov, Zh. Éksp. Teor. Fiz. **89**, 203 (1985) [Sov. Phys. JETP **62**, 115 (1985)].
[4] A. M. Balbashev, A. A. Volkov, S. P. Lebedev *et al.*, Zh. Éksp. Teor. Fiz. **88**, 974 (1985) [Sov. Phys. JETP **61**, 573 (1985)].
[5] N. K. Dan'shin, S. V. Zherlitsyn, S. S. Zvada *et al.*, Fiz. Tverd. Tela (Leningrad) **31**, 198 (1989) [Sov. Phys. Solid State **31**, 832 (1989)].
[6] V. É. Arutyunyan, K. N. Kocharyan, and R. M. Martirosyan, Zh. Éksp. Teor. Fiz. **96**, 1384 (1989) [Sov. Phys. JETP **69**, 783 (1989)].

[7] N. K. Dan'shin, Yu. I. Nepochatykh, and V. F. Shkar', Zh. Éksp. Teor. Fiz. **109**, 639 (1996) [JETP **82**, 341 (1996)].
[8] R. Wolfe, R. D. Pierce, M. Eibshutz, and J. W. Nielsen, Solid State Commun. **7**, 949 (1969).
[9] H. Ḳoshizaka, M. Hirano, T. Okida *et al.*, AIP Conf. Proc. **24**, 61 (1975).
[10] V. É. Arutyunyan, K. N. Kocharyan, R. M. Martirosyan *et al.*, Zh. Éksp. Teor. Fiz. **98**, 712 (1990) [Sov. Phys. JETP **71**, 398 (1990)].
[11] V. D. Buchel'nikov, N. K. Dan'shin, L. T. Tsymbal, and V. G. Shavrov, Usp. Fiz. Nauk **166**, 585 (1996).
[12] I. K. Dikshteĭn, V. V. Tarasenko, and V. G. Shavrov, Fiz. Tverd. Tela (Leningrad) **19**, 1107 (1977) [Sov. Phys. Solid State **19**, 644 (1977)].
[13] V. D. Buchel'nikov and V. G. Shavrov, JETP Lett. **60**, 548 (1994).
[14] V. D. Buchel'nikov and V. G. Shavrov, Zh. Éksp. Teor. Fiz. **106**, 1756 (1994) [JETP **79**, 951 (1994)].

Translated by M. E. Alferieff

Destruction of the ozone layer as a result of a meteoroid falling into the ocean

B. A. Klumov
Institute of the Dynamics of Geospheres, 117334 Moscow, Russia

(Submitted 1 July 1999; resubmitted 28 July 1999)
Pis'ma Zh. Éksp. Teor. Fiz. **70**, No. 5, 360–366 (10 September 1999)

The falling of a large celestial body into the ocean causes a large number of compounds (for example, HCl, Cl, Br, Na, H_2O, OH, and NO) that destroy ozone molecules directly or indirectly to be ejected to stratospheric altitudes. The bleaching of the atmosphere in the UV range as a result of such ozone destruction creates negative feedback that restores the ozone. The characteristic time for such restoration in the stratosphere decreases sharply with altitude, ranging from several months at 30 km to several days at 20 km. © *1999 American Institute of Physics.* [S0021-3640(99)00917-2]

PACS numbers: 92.70.Cp, 92.60.Hp, 96.50.Mt, 94.10.Fa

In the present letter the effect of the impact of a large celestial body on processes controlling the ozone level in the stratosphere is studied.

It is easy to estimate the minimum size r^{cr} of a meteoroid that reaches the Earth's surface: The mass of the air column drawn into motion as a result of the deceleration of a meteoroid in the atmosphere is of the order of the meteoroid mass, so that the atmosphere is ''transparent'' to meteoroids of size r_i greater than $r^{cr} \sim \rho_0 \rho_i^{-1} H_{char} \sin^{-1}\theta$, where ρ_i and ρ_0 are, respectively, the density of the meteoroid and of the Earth's atmosphere at the surface (H_{char} is the scale height of the atmosphere, $H_{char} \simeq 8$ km at stratospheric altitudes), and θ is the angle of entry of the meteoroid into the atmosphere. For the most probable angles of entry ($\theta \simeq 45°$) we obtain $r^{cr} \simeq 10$ m.

During the deceleration process a meteoroid is deformed by the airstream. In the hydrodynamic approximation the cross section for the interaction of the meteoroid with the atmosphere increases with density: $dr_i/dt \simeq v_i \sqrt{\rho(h)/\rho_i}$, where v_i is the meteoroid velocity. It is easy to show that in this case r^{cr} is much greater than for deceleration of a nondeformable meteoroid:

$$r^{cr} \simeq \frac{H_{char}}{\sin\theta} \sqrt{\frac{\rho_0}{\rho_i}} \simeq 200-300 \text{ m}$$

for asteroids ($\rho_i \simeq 2.5\ \text{g/cm}^3$) and comets ($\rho_i \simeq 1\ \text{g/cm}^3$), respectively. The mass of such a meteoroid is $M^{cr} \sim 10^{14}$ g.

Let us consider the response of the ozone layer to the falling of a meteoroid with $r_i \simeq r^{\rm cr}$ into the ocean. We note that the probability of such a meteoroid colliding with the earth is of the order of 10^{-4} yr^{-1} (Ref. 1). Without loss of generality, it can be assumed[1)] that $v_i \simeq 25$ km/s and $\rho_i \simeq 1$ g/cm^3. We shall consider the effect on the ozone of only the ocean water that can reach stratospheric altitudes in such an impact (i.e., we used the deep ocean approximation). We shall neglect the effects due to the presence of the ocean bottom. For sufficiently large meteoroids, this assumption breaks down, since the penetration depth d_p of a meteoroid into the ocean becomes greater than the ocean depth [for comets in a vertical impact $d_p \simeq (4-6) r_i$ (see, for example, Ref. 3)], and the soil matter together with water are ejected into the stratosphere. It should be noted that studies of the effect of the impact of a large celestial body on the surrounding medium have been concerned primarily with the change in the radiation balance (dust in the atmosphere, loading of the atmosphere with aerosols and greenhouse gases [CO_2, H_2O, CH_4, and others) and possible climate changes induced by the impact (see, for example, Ref. 4 and citations therein)]. However, in the present letter we consider the case where the radiation balance is destroyed as a result of the photochemical destruction of the ozone layer caused by ozone-active (ozone-destroying) compounds reaching the stratosphere after the impact. We shall consider the impact of meteoroids with $r_i \simeq r^{\rm cr}$, for which the deep-ocean approximation is quite justified.

Ocean water contains large quantities of ozone-active compounds, such as, for example, Na, Cl, and Br. The effect of the water is due to the possibility of its photodecomposition in the stratosphere by sunlight with formation of the ozone-active radical OH. However, nitric oxide NO, which effectively destroys ozone, can form behind the shock wave (SW) arising as the meteoroid decelerates in the atmosphere and in the process of supersonic ejection of impactor and target matter immediately after the impact.

The meteoroid track, in which large quantities of oxides of nitrogen are formed, could have a definite effect on stratospheric ozone. However, for not very large meteoroids the lifetime of the ozone depression caused by this track is short, and the impact vapor ejected into the stratosphere plays the key role. We shall show this.

The initial pressure p_0 in the meteoroid track is of the order of $(0.2-0.3)\rho_s v_i^2 \gg p_s$, where ρ_s and p_s are the density and pressure of the surrounding stratospheric air, the parameter $r_i v_i^2 / H_{\rm char} c_s^2 \gg 1$ for $r_i \sim r^{\rm cr}$, where c_s is the sound velocity in the stratosphere. This parameter is the ratio of the lifetime of a strong shock wave ($\tau \sim r_s / v_i \simeq (dE_i/dh)^{0.5} \rho_s^{-0.5} c_s^{-2} \simeq r_i v_i c_s^{-2}$, where r_s is the radius of the strong shock wave, and E_i is the energy of the meteoroid) to the characteristic stopping time ($\tau \sim H_{\rm char}/v_i$). For this reason, for the impact parameters considered, the expansion of the meteoroid track can be described in the approximation of a strong cylindrical explosion. In such an explosion the formation and quenching of nitric oxide (NO) occur behind the shock front.

The mass $M_{\rm NO}$ of the nitric oxide formed behind the shock front in the stratosphere as the meteoroid decelerates can be estimated from the relation

$$M_{\rm NO} \simeq \pi r_i^2 \delta_{\rm NO} \rho_s H_{\rm char}, \tag{1}$$

where $\delta_{\rm NO}$ is the relative NO content in the meteoroid track, which is ''frozen'' during rapid cooling of the shock-heated air. The time $\tau_{\rm NO}$ for the establishment of thermodynamic equilibrium for NO in hot air is determined (in the temperature range of interest to us 1500–2500 K; as will be shown below, the characteristic cooling time of the track is

comparable to the thermodynamic equilibration time of NO) by the reaction $NO + O_2 \rightarrow NO_2 + O$ with the rate constant $k_1 \simeq 3\times 10^{-12}\exp(-23400\,\mathrm{K}/T)$, and correspondingly $\tau_{NO} = (k_1[O_2])^{-1} \simeq 10^{-7}\exp(23400\,\mathrm{K}/T)\rho_0/\rho_s$. Here $[O_2]$ is the density of oxygen molecules at stratospheric altitudes; the fraction of molecular oxygen in air in the temperature range under consideration is $\simeq 0.2$. It is evident that τ_{NO} increases rapidly as the air cools; in the lower stratosphere, at altitudes $\simeq 20$ km, one has $\tau_{NO} \sim 0.01$ s at a temperature of 2500 K and $\tau_{NO} \sim 10$ s at 1500 K.

The quenching temperature T^q_{NO} of nitric oxide can be estimated from the relation $\tau_{NO}(T^q_{NO}, p_s) \simeq \tau_c$ where τ_c is the characteristic cooling time of hot air in the meteoroid track, $\tau_c \sim r_i/c_s$. The nitric oxide fraction δ_{NO} ''frozen'' during such expansion is close to the thermodynamically equilibrium fraction of NO at a temperature close to the quenching temperature and pressure p_s of the surrounding stratospheric air. In our case ($r_i \simeq r^{cr}$) $\tau_c \sim 0.3$ s, and $T^q_{NO} \sim 1750-2000$ K. At such temperatures the equilibrium NO content in air is approximately 1%. At stratospheric altitudes, such values of δ_{NO} correspond to nitric oxide densities $n^w_{NO} \simeq 10^{15}-10^{16}\,\mathrm{cm}^{-3}$. These are very high values, more than a million times higher than the background level of nitrogen oxides in the stratosphere ($n_{NO} + n_{NO_2} \simeq 10^9\,\mathrm{cm}^{-3}$).

Turbulent diffusion processes decrease the NO density in the meteoroid track, based on which an air column with a strongly nonequilibrium concentration of nitrogen oxides forms. The spatiotemporal parameters of such a column can be estimated on the basis of the diffusion equation whose solution, neglecting photochemical processes, is $n_{NO}(r,t) \propto \exp(-r^2/Kt)/t$, where K is the turbulent diffusion coefficient, which in the stratosphere is $K \simeq 8t^{1.6}\,\mathrm{cm}^2/\mathrm{s}$ (Ref. 5). The radial size of the column with strongly perturbed NO content is $r_{neq} \simeq 0.1 r_i \sqrt{n^w_{NO}/n^0_{NO}} \sim 100 r_i$. The characteristic lifetime τ_d of such a column with respect to diffusion spreading can be estimated from $r_{neq} \simeq \sqrt{K\tau_d}$, or $\tau_d \simeq 4\times 10^4$ s.

The excess NO produces a local depression of ozone via the reaction

$$NO + O_3 \rightarrow NO_2 + O_2 \tag{2}$$

with rate constant $k_2 \simeq 4\times 10^{-12}\exp(-1560\,\mathrm{K}/T)\,\mathrm{cm}^3/\mathrm{s}$.

At stratospheric altitudes $k_2 \simeq 4\times 10^{-15}\,\mathrm{cm}^3/\mathrm{s}$. Comparing the characteristic time τ_{oz} of ozone destruction in this reaction, $\tau_{oz} \simeq (k_2 n_{NO})^{-1}$, with τ_d we find that appreciable ozone destruction in the column under consideration starts at densities $n^{cr}_{NO} \geqslant 10^{11}\,\mathrm{cm}^{-3}$. The radial size r_{oz} of the column where ozone is virtually completely destroyed can be estimated as $r_{oz} \simeq r_i \sqrt{n^w_{NO}/n^{cr}_{NO}} \sim 100 r_i$.

Therefore, a local (with scale $\sim r_{oz}$) and transient (with characteristic lifetime $\sim \tau_d$) ozone depression is formed in the stratosphere on the basis of the meteoroid track. For the impact of a comet with $r_i \approx r^{cr}$ approximately $\pi r^2_{oz} H_{char} \rho_s \sim 10^9 - 10^{10}$ g ozone are destroyed in the comet track; this amount is not comparable to the total amount of ozone in the stratosphere ($\sim 10^{16}$ g).

Let us now consider the impact of a meteoroid ($r_i \simeq r^{cr}$, $v_i \simeq 25$ km/s) against the ocean surface. In such an impact, virtually complete vaporization of the impactor matter and vaporization of a substantial fraction of the target material occur, and the mixed multiphase impactor and target matter is ejected into the atmosphere. The mass m_{ej} of the matter ejected as a result of the impact can be estimated using the relation[6]

$$m_{ej}/m_i \simeq 0.2 \cdot \left\{ \frac{v_i^2}{g} (\rho_t/m_i)^{1/3} \right\}^{0.46}, \quad (3)$$

where g is the acceleration of gravity, m_i is the impactor mass, and ρ_t is the target density. We shall estimate the mass m_v of the vaporized ocean water using the relation[3] $m_v \simeq 0.2 \cdot m_i (v/\sqrt{Q_v \rho_t})^{1.4}$, where Q_v is the latent heat of vaporization of water. In our case $m_{ej} \sim 100 m_i$ and $m_v \sim 10 m_i \simeq 10^{15}$ g.

A substantial fraction of the ejected impact vapor easily reaches stratospheric altitudes. The initial velocity distribution over the radius r in the impact vapor cloud is close to linear: $v(r) \sim v_{\max} r/R_{\max}$, where $v_{\max}$ is the expansion velocity of the hot cloud and $v_{\max} \sim v_i/3 - v_i/4$ in our case. As long as the pressure in the cloud is much higher than the pressure of the surrounding air, the impact vapor cloud expands almost freely; its radius grows with time as $R_{\max} \simeq v_{\max} t$. It is obvious that almost the entire mass of the impact vapor can reach the stratospheric altitudes, since the velocity required for this is quite low ($\sim \sqrt{2gh} \ll v_{\max}$). Thus a meteoroid impact results in the ejection of an appreciable fraction of the target matter in the form of impact vapor into the upper atmosphere. For impacts with velocities $v_i \simeq 25$ km/s, which are characteristic for comets, $m_v \sim 10 m_i$. What is the composition of such an impact vapor?

Thermodynamic calculations show that the main compounds of the indicated impact vapor are H_2O (~90%), HCl (~1%), NaCl (~1%), OH (~0.2%), Cl (~0.01%), and NaOH (~0.01%). The uncertainty in the composition and amount of ejected impact vapor can result in appreciable uncertainty in the amount of ozone active compounds reaching the stratosphere as a result of the impact. For this reason, in our photochemical calculations we varied over wide limits the initial level of the ozone-destroying compounds that are added to the stratospheric gas as a result of the impact.

It is quite difficult to determine the amount of NO formed in the stratosphere as a result of a meteoroid impact; NO forms behind the shock front, both as a result of supersonic ejection of impact vapor into the stratosphere and when the ejected matter subsequently falls back onto the stratosphere. An upper limit of the NO mass formed as a result of ejection of the impact vapor, $M_{\rm NO}^{ej} \sim \rho_0 \delta_{\rm NO} H_{\rm char}^3 \sim 10^{12} - 10^{13}$ g, can be easily obtained if the mass of the air traversed by the shock wave is known. We note that in a meteoroid track with $r_i \simeq r^{\rm cr}$ substantially less nitrogen oxides are formed at stratospheric altitudes.

Nitric oxide can form behind a shock front as a result of the falling of the ejected matter back onto the atmosphere. The mass of the NO produced in this process can be estimated in the ballistic approximation as $M_{\rm NO}^{fb} \leqslant 0.1 m_i$. Indeed, using the cumulative distribution of the ejected matter over the velocities $M(>v) \propto v^{-\alpha}$ (with the normalization $M(>v) \simeq 0.1 m_i (v_i/v_{\max})^2 (v_{\max}/v)^{\alpha}$), where $M(>v)$ is the mass of the impact vapor with velocities greater than v, the exponent $\alpha \simeq 1.6$,[6] and since NO is formed only behind a sufficiently strong SW (with temperature $T_f \geqslant 2500$ K behind the front and, correspondingly, shock wave velocity $v_{\rm NO} \geqslant 2-3$ km/s), we obtain $M_{\rm NO}^{fb} \sim \delta_{\rm NO} M(>v_{\rm NO}) \sim 0.1 m_i$.

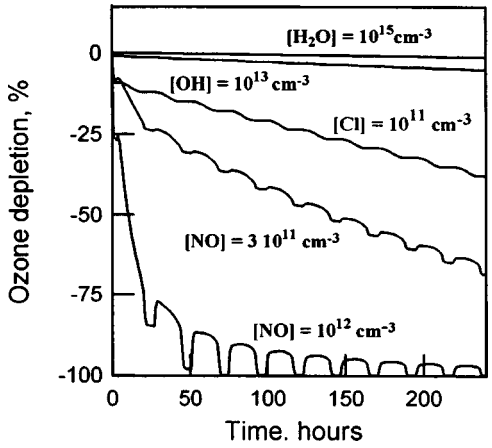

FIG. 1. Ozone destruction at an altitude of 20 km as a result of the injection of a various ozone-active compounds. The densities (in cm^{-3}) of the compounds added to the stratospheric air and the response of ozone to such an addition are indicated.

We shall now determine the characteristic scale of the perturbation in the stratosphere after the ejected impact vapor falls on it. The distribution of this material M_l as a function of distance l from the impact location is $M_l \sim v^{-1} M(>v)/(dl/dv)$. Since $l \simeq v^2 \sin 2\theta/g$, we immediately obtain $M_l \propto v^{-(\alpha+2)} \propto v^{-3.6} \propto l^{-1.8}$. The density ρ_{fb} of matter decreases rapidly with distance l: $\rho_{fb} \propto M_l/l \propto l^{-2.8}$, and the pressure in the shock wave from the falling gas decreases with distance l as $p_{fb} \propto \rho_{fb} v^2 \propto l^{-1.8}$. The characteristic scale l_s of the region of the atmosphere where the composition of the atmosphere strongly perturbed by the ejected gas and the indicated gas forms a shock wave in the stratosphere can be determined from $l_s \sim (m_i L_{\max}^{0.8}/\rho_s H_{\text{char}})^{1/2.8} \sim 100$ km, and the dependence $\rho_{fb}(l)$ acquires the form $\rho_{fb}(l) \simeq \rho_s (l_s/l)^{2.8}$. The amount of NO formed behind the shock front as the ejected impact vapor falls onto the atmosphere can be estimated as $M_{\text{NO}}^{fb} \sim \pi l_s^2 H_{\text{char}} \delta_{\text{NO}} \rho_s \sim 10^{13} - 10^{14}$ g for a comet with $r_i \simeq r^{\text{cr}}$, which agrees with the estimate presented above. The scale l_{oz} of the stratospheric region where the level of ozone-active compounds is much higher than the background values is much greater than l_s: $l_{\text{oz}} \sim l_s (\rho_s/10\delta)^{1/2.8} \sim 1000$ km, where $\delta \sim 10^{-8}$ is the background fraction of ozone-active compounds in the stratosphere.

In summary, after the impact of a meteoroid with $r_i \geqslant r^{\text{cr}}$ a ''spot'' of size $2l_{\text{oz}}$, where the air composition is strongly perturbed and the impact vapor material is added to the air, forms in the stratosphere. The characteristic densities n_j of ozone-active compounds in the ''spot'' are $n_j \sim M_i N_A (\pi l_s^2 H_{\text{char}} \mu_j)^{-1}$; for NO and Cl $n_{\text{Cl}} \sim n_{\text{NO}} \sim 10^{12}\,\text{cm}^{-3}$.

Let us consider the photochemical consequences of such an addition and primarily its effect on the ozone. We note that the characteristic lifetime of such a ''spot''[2)] in the stratosphere with respect to spreading as a result of atmospheric dynamics processes is $\sim l_s^2/K$ and is much greater than the characteristic time of significant photochemical processes.

Figure 1 shows the time dependences of the ozone concentration at 20 km altitude

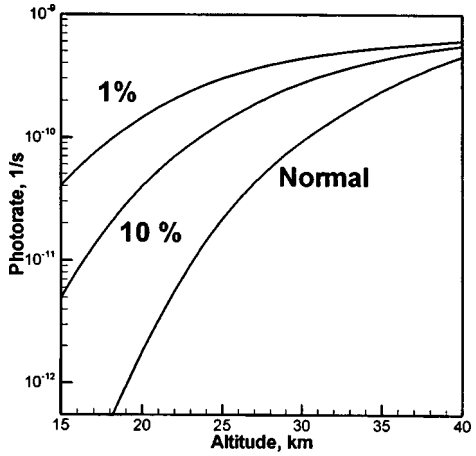

FIG. 2. Photodissociation rate J_{O_2} of molecular oxygen O_2 versus the altitude for different degrees of ozone destruction. The solar zenith angle is 45°. The dependences of J_{O_2} for normal conditions and for an ozone layer in which 10% and 1% ozone remain are shown.

with the addition of a number of ozone-active compounds to the standard composition of the air at this altitude. The numerical results presented are based on our photochemical model of stratospheric ozone.[8] Note the weak response of ozone to the addition of water and the hydroxyl radical OH. This is due to the rapid conversion of excess hydroxyl into water via the formation of hydrogen peroxide H_2O_2. The addition of nitric oxide or chlorine is a threshold-like process — for large initial disturbances of their densities ($\sim 10^{11}-10^{12}\,\mathrm{cm}^{-3}$, which corresponds to δ^d_{Cl}, $\delta^d_{\mathrm{NO}}\sim 10^{-7}-10^{-6}$) ozone is destroyed comparatively rapidly (within several hours) and switches into a regime with strong daily variations (under ordinary conditions such variations in the stratosphere are negligible) with maximum value $\sim$1% of the normal ozone level ($\sim 10^{12}\,\mathrm{cm}^{-3}$, $\delta_{\mathrm{O_3}}\sim 10^{-6}$).

Thus, the falling of a celestial body into the ocean can produce in the stratosphere a long-lived ''spot'' where ozone is virtually completely destroyed. Since the characteristic size of a such a ''spot'' is much greater than the scale height of the atmosphere, the change induced in the UV transparency of air by the destruction of the ozone must be taken into account in order to describe correctly the photochemistry inside the ''spot.'' The destruction of ozone on such spatial scales results in bleaching of the atmosphere in the UV range, which produces a negative feedback that restores the ozone. This effect is illustrated in Fig. 2, which shows the altitude profiles of the photodissociation rate of molecular oxygen O_2 for various levels of the ozone depression in the stratosphere. To calculate the photodissociation rate we solved the transfer equation for sunlight in the Earth's atmosphere numerically using the Phodis code.[9] We note that oxygen atoms are formed in the process of the photodestruction of O_2, and these atoms form ozone in the three-body recombination reaction $O+O_2+M\rightarrow O_3+M$. All other significant rates of photoprocesses remain virtually unchanged — these compounds do not require for their photodecomposition[3)] the hard UV radiation required for photodissociation of O_2.

In the lower stratosphere the effect can be very substantial: the O_2 photodissociation rate J_{O_2} in the ''spot'' can be a hundred times higher than the ordinary level. This results

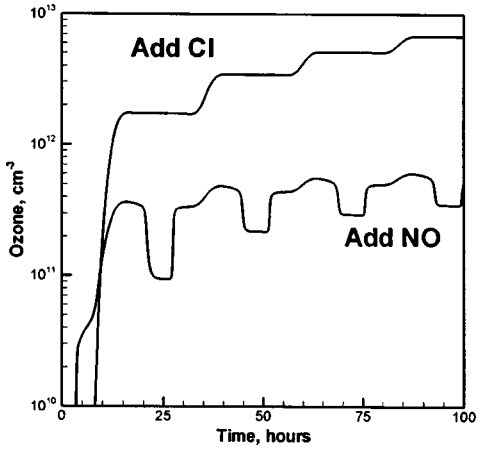

FIG. 3. Ozone restoration at 20 km with almost complete destruction of the ozone after the injection of Cl and NO. The destruction of the ozone results in a sharp increase in ozone formation rate as a result of an increase in the UV flux.

in restoration of ozone in the ''spot'' at a rate $\sim J_{O_2}(h)[O_2](h)$. The characteristic time τ_r of such restoration at an altitude of 20 km is of the order of $10n_{O_3}(J_{O_2}[O_2])^{-1} \simeq 10^5$ s. Figure 3 shows such the restoration of ozone at 20 km, observed immediately after the destruction of the ozone and the resulting increase in the UV flux. We note that ozone is restored at different rates at different altitudes: In the lower stratosphere ($h \simeq 20$ km) $\tau_r \sim 10^5$ s, whereas at altitudes $h \simeq 30$ km the restoration time is much longer: $\tau_r \sim 10^7$ s — a wave of ''ozone restoration'' travels from bottom to top along the perturbed stratosphere.

In summary, the falling of a celestial body into the ocean results in a number of little-studied effects. A substantial quantity of ozone-destroying compounds enters the stratosphere as a result of such an event. The ozone destruction results in a sharp increase in the rate of photodissociation of molecular oxygen, which in turn results in rapid restoration of ozone. This effect is especially large in the lower stratosphere, where the ozone restoration time is of the order one day. In this connection, it would be interesting to investigate how this effect influences the polar ozone hole. It is easy to show that the effect considered above is negligible in this case. This is because the ozone hole in polar regions exists under the conditions of large zenith angles, which naturally decreases the effectiveness of UV radiation as an indirect source of ozone. Moreover, the polar ozone hole is formed primarily in the lower stratosphere at altitudes 15–20 km, while the ozone layer above this altitude is not disturbed much and appreciably attenuates the solar UV radiation, without creating in the process appreciable bleaching of the stratosphere in the UV range.

The effect considered above demands that the existing views of ozone destruction during catastrophic events be re-examined. This work was supported in part by the Russian Fund for Fundamental Research (Grant No. 99-02-16938).

[1)]According to Ref. 2, the most likely impact velocity for short-period comets colliding with the earth is close to 25 km/s. For asteroids it is much lower, approximately 12 km/s.
[2)]As a result of the comet SL9 falling into Jupiter's atmosphere, a ~6000 km ''spot'' formed in Jupiter's atmosphere. The characteristic lifetime of the spot was $\sim 3\times 10^6$ s. The evolution of this ''spot,'' which converted into a relatively stable vortex, gradually dissipated by zonal flows, was simulated in Ref. 7.
[3)]A large increase in the rate of photodissociation of NaCl as a result of ozone destruction can lead, in turn, to an increase in the ozone restoration time. This question falls outside the scope of the present letter.

[1] C. R. Chapman and D. Morrison, Nature (London) **367**, 33 (1994).
[2] C. F. Chyba, Icarus **92**, 217 (1991).
[3] T. J. Ahrens, J. D. O'Keefe, J. Geophys. Res. Suppl. **88**, 799 (1983).
[4] O. B. Toon, K. Zahnle, R. P. Turco *et al.*, Reviews of Geophys. **35**, 1, 41 (1997).
[5] *The Natural Stratosphere*, CIAP Monograph, Washington, 1975.
[6] C. F. Chyba, T. C. Owen, W. H. Ip, in *Hazards due to Comets and Asteroids*, edited by T. Gehrels (University of Arizona Press, 1994), p. 9.
[7] V. E. Fortov, Yu. N. Gnedin, M. F. Ivanov *et al.*, Usp. Fiz. Nauk **166**, 391 (1996).
[8] B. A. Klumov, Geophys. Res. Lett. (in preparation), 1999.
[9] A. Kylling, Phodis code, http://kaja.gi.alaska.edu.

Translated by M. E. Alferieff